Received: 26 October 2020 | Revised: 21 January 2021 | Accepted: 16 February 2021

DOI: 10.1002/nme.6660

RESEARCH ARTICLE

WILEY

Structural analysis of composite tubes using a meshless analytical dimensional reduction method

Saeid Khadem Moshir | **Suong Van Hoa** | **Farjad Shadmehri**

Concordia Center for Composites (CONCOM) Department of Mechanical, Industrial and Aerospace Engineering, Concordia University, Montreal, Quebec, Canada

Correspondence
Suong Van Hoa, Concordia Center for Composites (CONCOM) Department of Mechanical, Industrial and Aerospace Engineering, Concordia University, Montreal, Quebec, Canada.
Email: hoasuon@alcor.concordia.ca

Funding information
Bell Flight; Natural Sciences and Engineering Research Council of Canada (NSERC) through the Industrial Research Chair on Automated Composites Manufacturing

Abstract

A polynomial-based model in conjunction with dimensional reduction method are presented to perform cross-sectional analysis and to determine strain distribution in composite tubes under bending loading. For beam structures with tubular cross-section, the Variational Asymptotic Method (VAM) has been employed to decompose a three-dimensional (3D) elasticity problem into a two-dimensional cross-sectional analysis and a one-dimensional analysis along the length. This greatly reduces computational time as compared to 3D Finite Element Method (FEM). There also exists publically available Variational Asymptotic Beam Sectional Analysis (VABS), a FEM cross-sectional analysis tool based on VAM. For VABS, FEM mesh for the beam section needs to be generated. For the case of composite tubes with many layers, the mesh generation consumes efforts and is unnecessary. We introduce a new meshless dimensional reduction method for the analysis of composite tubes. This method utilizes Pascal polynomials in polar coordinates to model the warping functions. Using this, one can obtain stiffness constants and 3D strains of the composite tube. This method is straightforward, meshless, with similar computation time as VABS, and is much more efficient than conventional 3D FEM. The accuracy of the proposed method is examined by comparing the obtained results with 3D FE (ANSYS), VABS, literature, and experiment.

KEYWORDS

classical beam model, composite tubular beams, finite element method, Timoshenko beam model, variational asymptotic beam sectional analysis, variational asymptotic method

1 | INTRODUCTION

The application of composite structures in the aerospace industry has attracted increasing interest in the last few decades due to their high strength to weight ratio. The motivation of this study comes from the need to find fast calculation methods to determine the deformation of thick composite tubular beams (more than 50 layers) subjected to three-point or four-point bending loading conditions. These composites tubular beams are intended to be used as cross piece of landing gear for helicopters.[1] One way to perform the stress analysis of these structures is three-dimensional (3D) Finite Element Analysis (FEA). However, this method is very time consuming. In order to have a good accuracy, each layer thickness

should be modeled using one element. For a structure containing 50 layers or more, with a cross-section diameter of about 50 mm and a length of about 1200 mm, the number of elements can go up to several hundred thousand elements. In one case study (shown in Section 5.3.1 in this paper), using ANSYS (commercial software) 3D FE requires 3192 k elements with a computer run time of 55 mi, while similar results can be obtained within 15 s using a more efficient method (also presented later in this paper).

For structures where there exists one (or two) dimensions (such as thickness or radius of the cross-section) that are much smaller than the other dimension (such length), one approach to reduce the computation effort in deformation analysis is the dimensional reduction method. Many previous researchers have used this approach.

Giavotto et al.[2] presented a numerical dimensional reduction method based on FE for cross-sectional discretization of an arbitrary cross-section of a beam. They extracted a 6×6 stiffness matrix of the cross-section with considering the shear effects. They developed a computer code HANBA2. Borri et al[3] extended the application of the method by Giavotto et al. to the case of naturally curved and twisted beams. The most significant work in the analysis of composite beams based on FE was developed by Hodges et al.[3-5] The Variational Asymptotic Method (VAM) is employed to minimize the energy functional of the beam. Hence, there is no ad hoc assumption in the 3D beam analysis. The approach includes all the non-classical effects and splits the original 3D geometrically nonlinear problem of a beam into a one-dimensional (1D) global beam analysis and a two-dimensional (2D) cross-sectional analysis. Generally, based on first and second approximations of the strain energy, a certain beam model is obtained including classical beam model which is represented by a 4×4 stiffness matrix without effects of transverse shears, and a generalized Timoshenko beam model which leads to a 6×6 stiffness matrix which takes into account transverse shear effect.[6,7] Berdichevsky et al.,[8] applied VAM to cross-sectional analysis of thin-walled anisotropic beams which led to a closed-form solution for the 4×4 stiffness matrix. Hodges et al.[9] used VAM to analyze of initially curved and twisted composite beams. The FEM is used to solve the nonlinear equations for nonlinear static deformation and linearized free vibration about the static state of the deformation. Popescu and Hodges[10] presented a FE cross-sectional analysis of beams which accounts for shear effects using VAM. Both the classical as well as Timoshenko beam models results for different cases of cross-section geometry have been presented.

A FE-based computer code called Variational Asymptotic Beam Sectional Analysis (VABS) was developed for 2D analysis based on VAM.[11] VABS extracts cross-sectional stiffness constants needed for 1D analysis of a FEA software. It also carries out recovery solution to provide stress and strain contour distribution in the cross-section.[4,7] It uses 2D FE for the cross-sectional analysis. The computational time is decreased considerably compared to 3D FE analysis.[11] This can be considered as the main advantage of the VABS over 3D FE analysis.

In the case of dimensional reduction method for tubular cross-sections using VAM, several works have been carried out. Based on the Timoshenko refinement of the VAM, Popescu and Hodges[10] compared the obtained stiffness constants of a composite Circumferentially Uniform Stiffness (CUS) beam using FE for cross-sectional discretization with those obtained Rehfield et al.[12] in which they used nonclassical beam theory. Ghafari and Rezaeepazhand[13] applied dimensional reduction method to obtain a 4×4 classical beam model stiffness matrix of an isotropic circular cross-section using Nonuniform Rational B-spline for cross-sectional discretization. They also applied the method to composite box beams. Jiang and Yu[14] developed nonlinear cross-sectional analysis of a hyperelastic material under finite deformation using VABS. They studied structural behavior of a composite pipe consisting of two layers, and having cross section in the form of a box beam with rounded ends.

Previous work as seen from the literature for the stress analysis of composite tubular beams has focused on beams with fairly complex geometries sch as composite box beams. For such structure, the use of FE to mesh the complex geometry of the cross-section is essential. For circular sections, such as that of the cross tube used for helicopters or similar structures, the use of FE to mesh the cross-section may not be necessary. The use of a simpler method may facilitate simpler input, and better insight into the understanding of the behavior of the structure. This is the objective of the current paper. That is to use the procedure of the VAM so that dimensional reduction is exploited to reduce the computational effort, but not using the FE meshing of the VABS. Rather, the warping function for the deformation of the section is represented by a polynomial (Pascal polynomial) in polar coordinates. Since no meshing is required, it is termed a "meshless" method.

In order to introduce the Pascal polynomial method, due to the complexity of the procedure, some aspects of the VAM is represented here for clarity and completeness.

2 | VAM PROCEDURE

The VAM consists of many steps. Details of the steps are presented below.

2.1 | Step 1: Identification of small parameters and formulation for 3D strains

In step 1, three aspects are considered. One is the identification of the small parameters essential for the application of VAM. The small parameters are the maximum of the axial strain ϵ_{max} and the thickness-to-radius ratio (h/r_o) and the radius-to-length ratio (r_o/L).[15] It is assumed that the $h/r_o \ll 1$ and $r_o/L \ll 1$. So that once can conclude that $h/L \ll 1$ and the ratio between the small dimension and the large dimension (h/L) of the structure, where h can be the thickness or diameter of the section, and L is the length. The other aspect is the formulation to obtain relations between the 3D strains in terms of warping functions and the 1D strains, using vector mechanics. According to kinematics of the beam deformation presented by Yu et al.[4] based on the decomposition of the rotation tensor, the 3D strain field for a beam without initial twist and curvature can be written the following form.

$$\mathbf{\Gamma} = [\Gamma_{11}\ 2\Gamma_{12}\ 2\Gamma_{13}\ \Gamma_{22}\ 2\Gamma_{23}\ \Gamma_{33}]^T \tag{1}$$

where 1, 2, and 3 refer to the x_1, x_2, x_3 coordinate axes as shown in Figure 2, respectively. This 3D strain can be considered as follows.

$$\mathbf{\Gamma} = [\Gamma_h]\boldsymbol{w} + [\Gamma_\epsilon]\overline{\boldsymbol{\epsilon}} + [\Gamma_l]\boldsymbol{w}' \tag{2}$$

where

$$[\Gamma_h] = \begin{bmatrix} 0 & 0 & 0 \\ \frac{\partial}{\partial x_2} & 0 & 0 \\ \frac{\partial}{\partial x_3} & 0 & 0 \\ 0 & \frac{\partial}{\partial x_2} & 0 \\ 0 & \frac{\partial}{\partial x_3} & \frac{\partial}{\partial x_2} \\ 0 & 0 & \frac{\partial}{\partial x_3} \end{bmatrix}, [\Gamma_\epsilon] = \begin{bmatrix} 1 & 0 & x_3 & -x_2 \\ 0 & -x_3 & 0 & 0 \\ 0 & x_2 & 0 & 0 \\ 0 & 0 & 0 & 0 \\ 0 & 0 & 0 & 0 \\ 0 & 0 & 0 & 0 \end{bmatrix}, [\Gamma_l] = \begin{bmatrix} [I]_3 \\ [O]_3 \end{bmatrix} \tag{3}$$

where, $[I]$ is the identity matrix and $[O]$ is the null matrix. The 1D strains of the reference line $\overline{\epsilon}$ can be expressed as the following

$$\overline{\boldsymbol{\epsilon}} = [\overline{\gamma}_{11}\ \ \overline{\kappa}_1\ \ \overline{\kappa}_2\ \ \overline{\kappa}_3]^T \tag{4}$$

where $\overline{\boldsymbol{\epsilon}}$ is strain vector of the reference line, which consists of the extensional strain $\overline{\gamma}_{11}$, the twist about the axis x_1 ($\overline{\kappa}_1$), bending curvature about the axis x_2 ($\overline{\kappa}_2$), and bending curvature about axis x_3 ($\overline{\kappa}_3$). w is the warping function displacements of the cross-section of the beam, which can be written in terms of its components as

$$\boldsymbol{w} = [w_1\ w_2\ w_3]^T \tag{5}$$

where w_1 represents the out-of-plane warping displacement at points on the cross-section in direction x_1, w_2, and w_3 are in-plane warping displacements of an arbitrary point in directions x_2 and x_3, respectively. The calculated warping functions in terms of the 1D strains of the reference line of the beam results in the transformation of the 3D model into a 1D beam model which maintains the 3D effects. Using the 3D strain field above, the dimensional reduction process can be performed. $\boldsymbol{w}'$ the partial derivative of $\boldsymbol{w}$ with respect to x_1 as shown in Figure 1.

2.2 | Step 2: Strain energy expression

In step 2, 3D strain energy expressions are formulated, first in terms of the 3D strains, and then in terms of the 1D strain and curvature of the reference line. The strain energy of the beam U can be expressed as[6]

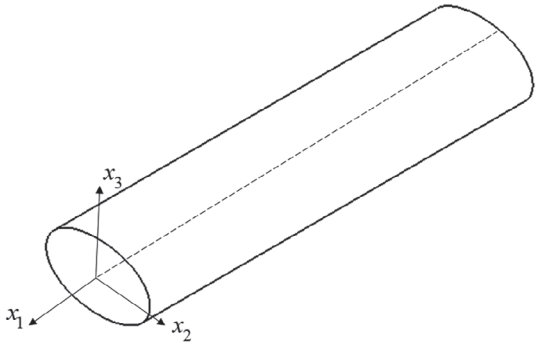

FIGURE 1 Beam and its coordinates

$$2U = \int_L \iint_\Omega \mathbf{\Gamma}^T [D] \mathbf{\Gamma} dx_2 dx_3 dx_1$$
$$= \int_L \iint_\Omega ([\Gamma_h]\boldsymbol{w} + [\Gamma_\epsilon]\overline{\boldsymbol{\epsilon}} + [\Gamma_l]\boldsymbol{w}')^T [D] ([\Gamma_h]\boldsymbol{w} + [\Gamma_\epsilon]\overline{\boldsymbol{\epsilon}} + [\Gamma_l]\boldsymbol{w}') dx_2 dx_3 dx_1 \tag{6}$$

where Ω is the cross-sectional area. $[D]$ is the matrix of material stiffness which carries the information of the material property and fiber orientation and layer orientation.

2.3 | Step 3: Assumption for the warping field of the cross-section

In Equation (6), the unknowns are the warping functions $w(x_1, x_2, x_3)$, and the strains of the reference line $\overline{\boldsymbol{\epsilon}}$. The VABS approach to provide solution is to assume that the warping function is a product two entities, one is some function of x_2 and x_3, and the other is function of only on x_1.

The warping field is discretized as

$$\boldsymbol{w}(x_1, x_2, x_3) = [W(x_2, x_3)]\boldsymbol{V}(x_1) \tag{7}$$

where $[W(x_2, x_3)]$ is the matrix of finite element shape functions, and $\boldsymbol{V}(x_1)$ as a column vector of the nodal values of the warping displacement over the cross-section in VABS method.

2.4 | Step 4: Asymptotically correct refined theory

According to the VAM, we now consider the perturbation in the warping field as follows.[16]

$$\boldsymbol{w} = \underbrace{\boldsymbol{w}_0}_{\epsilon_{\max}} + \underbrace{\boldsymbol{w}_1}_{\epsilon_{\max} h/L} \tag{8}$$

where $\boldsymbol{w}_0$ has the order of $\epsilon_{\max}$ and $\boldsymbol{w}_1$ has the order of $\epsilon_{\max} h/L$. We can write

$$\boldsymbol{w}_0 = \underbrace{[W]\boldsymbol{V}_0}_{\epsilon_{\max}}, \boldsymbol{w}_1 = \underbrace{[W]\boldsymbol{V}_1}_{\epsilon_{\max} h/L} \tag{9}$$

and,

$$\boldsymbol{V} = \boldsymbol{V}_0 + \boldsymbol{V}_1 \tag{10}$$

Therefore, the strain field in Equation (2) can be expressed as

$$\boldsymbol{\Gamma} = \underbrace{[\Gamma_\epsilon]\overline{\boldsymbol{\epsilon}}}_{\epsilon_{\max}} + \underbrace{[\Gamma_h][W]\boldsymbol{V}_0}_{\epsilon_{\max}} + \underbrace{[\Gamma_h][W]\boldsymbol{V}_1}_{\epsilon_{\max}h/L} + \underbrace{[\Gamma_l][W]\boldsymbol{V}_0{}'}_{\epsilon_{\max}h/L} + \underbrace{[\Gamma_l][W]\boldsymbol{V}_1{}'}_{\epsilon_{\max}(h/L)^2} \tag{11}$$

In the strain field of Equation (11), the first and second terms have the order of $\epsilon_{\max}$, the third and fourth terms have the order of $\epsilon_{\max}h/L$ and the last term has the order of $\epsilon_{\max}(h/L)^2$. By considering Equations (10, 11) and Equation (6), the strain energy per unit length can be expressed as follows.

$$\begin{aligned}
2U = \int_L & \underbrace{(\boldsymbol{V}_1^T[D_{hh}]\boldsymbol{V}_1}_{\epsilon_{\max}^2h^2/L^2} + \underbrace{\overline{\boldsymbol{\epsilon}}^T[D_{\epsilon\epsilon}]\overline{\boldsymbol{\epsilon}}}_{\epsilon_{\max}^2} + \underbrace{\boldsymbol{V}_0^T[D_{hh}]\boldsymbol{V}_0}_{\epsilon_{\max}^2} + \underbrace{\boldsymbol{V}_0'^T[D_{ll}]\boldsymbol{V}_1{}'}_{\epsilon_{\max}^2h^3/L^3} + \underbrace{\boldsymbol{V}_1'^T[D_{ll}]\boldsymbol{V}_1'}_{\epsilon_{\max}^2h^4/L^4} \\
& + \underbrace{\boldsymbol{V}_1'^T[D_{ll}]\boldsymbol{V}_0'}_{\epsilon_{\max}^2h^3/L^3} + \underbrace{\boldsymbol{V}_1^T[D_{hh}]\boldsymbol{V}_0}_{\epsilon_{\max}^2h/L} + \underbrace{\boldsymbol{V}_0^T[D_{hh}]\boldsymbol{V}_1}_{\epsilon_{\max}^2h/L} + \underbrace{\boldsymbol{V}_0'^T[D_{ll}]\boldsymbol{V}_0'}_{\epsilon_{\max}^2h^2/L^2} + \underbrace{\overline{\boldsymbol{\epsilon}}^T[D_{h\epsilon}]\boldsymbol{V}_1}_{\epsilon_{\max}^2h/L} + \underbrace{\overline{\boldsymbol{\epsilon}}^T[D_{h\epsilon}]\boldsymbol{V}_0}_{\epsilon_{\max}^2} \\
& + \underbrace{\overline{\boldsymbol{\epsilon}}^T[D_{l\epsilon}]\boldsymbol{V}_1'}_{\epsilon_{\max}^2h^2/L^2} + \underbrace{\boldsymbol{V}_0^T[D_{h\epsilon}]\overline{\boldsymbol{\epsilon}}}_{\epsilon_{\max}^2} + \underbrace{\boldsymbol{V}_0^T[D_{hl}]\boldsymbol{V}_0{}'}_{\epsilon_{\max}^2h/L} + \underbrace{\boldsymbol{V}_0^T[D_{hl}]\boldsymbol{V}_1{}'}_{\epsilon_{\max}^2h^2/L^2} + \underbrace{\boldsymbol{V}_1^T[D_{h\epsilon}]\overline{\boldsymbol{\epsilon}}}_{\epsilon_{\max}^2h/L} + \underbrace{\boldsymbol{V}_1^T[D_{hl}]\boldsymbol{V}_0{}'}_{\epsilon_{\max}^2h^2/L^2} \\
& + \underbrace{\boldsymbol{V}_1^T[D_{hl}]\boldsymbol{V}_1{}'}_{\epsilon_{\max}^2h^3/L^3} + \underbrace{\boldsymbol{V}_0'^T[D_{l\epsilon}]\overline{\boldsymbol{\epsilon}}}_{\epsilon_{\max}^2h/L} + \underbrace{\boldsymbol{V}_0'^T[D_{hl}]\boldsymbol{V}_0}_{\epsilon_{\max}^2h/L} + \underbrace{\boldsymbol{V}_0'^T[D_{hl}]\boldsymbol{V}_1}_{\epsilon_{\max}^2h^2/L^2} + \underbrace{\boldsymbol{V}_1'^T[D_{l\epsilon}]\overline{\boldsymbol{\epsilon}}}_{\epsilon_{\max}^2h^2/L^2} + \underbrace{\boldsymbol{V}_1'^T[D_{hl}]\boldsymbol{V}_0}_{\epsilon_{\max}^2h^2/L^2} \\
& + \underbrace{\boldsymbol{V}_1'^T[D_{hl}]\boldsymbol{V}_1}_{\epsilon_{\max}^2h^3/L^3} + \underbrace{\overline{\boldsymbol{\epsilon}}^T[D_{l\epsilon}]\boldsymbol{V}_0'}_{\epsilon_{\max}^2h/L}dx_1
\end{aligned} \tag{12}$$

where the matrices $[D_{hh}]$, $[D_{h\epsilon}]$, $[D_{\epsilon\epsilon}]$, $[D_{hl}]$, $[D_{l\epsilon}]$, and $[D_{ll}]$ carry the information on the material properties and geometry of the cross-section as

$$\begin{aligned}
[D_{hh}] &= \int_{x_3}\int_{x_2}[\Gamma_hW]^T[D][\Gamma_hW]dx_2dx_3, \quad [D_{h\epsilon}] = \int_{x_3}\int_{x_2}[\Gamma_hW]^T[D][\Gamma_\epsilon]dx_2dx_3 \\
[D_{hl}] &= \int_{x_3}\int_{x_2}[\Gamma_hW]^T[D][\Gamma_lW]dx_2dx_3, \quad [D_{\epsilon\epsilon}] = \int_{x_3}\int_{x_2}[\Gamma_\epsilon]^T[D][\Gamma_\epsilon]dx_2dx_3 \\
[D_{ll}] &= \int_{x_3}\int_{x_2}[\Gamma_lW]^T[D][\Gamma_lW]dx_2dx_3, \quad [D_{l\epsilon}] = \int_{x_3}\int_{x_2}[\Gamma_lW]^T[D][\Gamma_\epsilon]dx_2dx_3
\end{aligned} \tag{13}$$

2.5 | Step 5: First and second approximation of the strain energy

The expression of the energy in Equation (12) has terms of different orders. By dropping terms of smaller magnitudes, different levels of solution can be obtained.

2.5.1 | First approximation

The first approximation in the warping field in the VAM comes from keeping the terms up to order $\epsilon_{\max}^2$ in the strain energy of Equation (12). Therefore, the order-zero of the linear strain density is as follows.

$$2U_0 = \int_L (\boldsymbol{V}_0^T[D_{hh}]\boldsymbol{V}_0 + 2\boldsymbol{V}_0^T[D_{h\epsilon}]\overline{\boldsymbol{\epsilon}} + \overline{\boldsymbol{\epsilon}}^T[D_{\epsilon\epsilon}]\overline{\boldsymbol{\epsilon}})dx_1 \tag{14}$$

The strain energy in Equation (14) is minimized with respect to the unknown warping $\boldsymbol{V}_0$using the following relation.

$$\frac{\partial U_0}{\partial \boldsymbol{V}_0} = 0 \tag{15}$$

This yields the classical beam model in which the effects of transverse shear are neglected. Substituting Equation (14) into Equation (15) leads to

$$[D_{h\epsilon}]\overline{\boldsymbol{\epsilon}} + [D_{hh}]\boldsymbol{V}_0 = 0 \tag{16}$$

Therefore, the unknown warping coefficients according to the order-zero of the strain energy is obtained as

$$\boldsymbol{V}_0 = -[D_{hh}]^{-1}[D_{h\epsilon}]\overline{\boldsymbol{\epsilon}} \equiv [\widehat{V}_0]\overline{\boldsymbol{\epsilon}} \tag{17}$$

It is difficult to invert the matrix $[D_{hh}]$ in Equation (17). To find the inverse of this matrix, a mathematical Pseudo method[17] is used. Using the obtained column matrix of Equation (17) and the order-zero of the strain energy Equation (14), the first approximation of strain energy and stiffness constants of the classical beam model can be achieved as follows.

$$2U_0 = \int_L (\overline{\boldsymbol{\epsilon}}^T([\widehat{V}_0]^T[D_{h\epsilon}] + [D_{\epsilon\epsilon}])\overline{\boldsymbol{\epsilon}})dx_1 = \int_L \overline{\boldsymbol{\epsilon}}^T[\overline{S}]\overline{\boldsymbol{\epsilon}}dx_1 \tag{18}$$

where $\overline{S}$ is a 4×4 stiffness matrix that expresses the beam cross-sectional stiffness coefficients. For a cross-section with area Ω, second moment of inertia I, polar moment of inertia J, elastic modulus E and shear modulus G, the stiffness constant $\overline{S}_{11}$ or $(E\Omega)$ is extensional stiffness, $\overline{S}_{22}$ or (GJ) is torsional stiffness, $\overline{S}_{33}$ or $(EI)_{x_2}$ and $\overline{S}_{44}$ or $(EI)_{x_3}$ are cross-sectional bending stiffness about x_2 and x_3 coordinates, respectively. Moreover, $\overline{S}_{12}$ is the extension-twist coupling, $\overline{S}_{13}$ and $\overline{S}_{14}$ are the extension-bending coupling stiffness. In the case of isotropic material, the cross-sectional stiffness matrix can be in the form expressed in (A1).

2.5.2 | Second approximation

The first approximation which leads to the classical beam model may not be accurate sufficiently for analysis of composite tubular beams with various lay-ups through the section. The second approximation of the strain energy with considering the transverse shear effect (Timoshenko refinement) may be accurate to predict the behavior of composite tubes. The strain energy up to order $O(\epsilon_{\max}^2 h^2/L^2)$ can be written as

$$\begin{aligned} 2U_1 = \int_L (&\boldsymbol{V}_1^T[D_{hh}]\boldsymbol{V}_1 + \overline{\boldsymbol{\epsilon}}^T[D_{\epsilon\epsilon}]\overline{\boldsymbol{\epsilon}} + \boldsymbol{V}_0^T[D_{hh}]\boldsymbol{V}_0 + \boldsymbol{V}'^T_0[D_{ll}]\boldsymbol{V}'_0 + 2\boldsymbol{V}_0^T[D_{h\epsilon}]\overline{\boldsymbol{\epsilon}} \\ &+ 2\boldsymbol{V}'^T_0[D_{l\epsilon}]\overline{\boldsymbol{\epsilon}} + 2\boldsymbol{V}'^T_1[D_{l\epsilon}]\overline{\boldsymbol{\epsilon}} + 2\boldsymbol{V}'^T_0[D_{hl}]\boldsymbol{V}_0 + 2\boldsymbol{V}_0^T[D_{hl}]\boldsymbol{V}'_1 + 2\boldsymbol{V}'^T_0[D_{hl}]\boldsymbol{V}_1)dx_1 \end{aligned} \tag{19}$$

It is noted that in the equation above the terms $2\boldsymbol{V}_0^T[D_{hh}]\boldsymbol{V}_1$ and $2\boldsymbol{V}_1^T[D_{h\epsilon}]\overline{\boldsymbol{\epsilon}}$ cancel out each other.[16] Also, in Equation (19), the term $\boldsymbol{V}_0^T[D_{hh}]\boldsymbol{V}_0$ is not mentioned in the strain energy obtained by Hodges.[3] However, this term is too low order. Integrating by parts of Equation (19) leads to Equation (20) as follows.

$$\begin{aligned} 2U_1 = \int_L (&\boldsymbol{V}_1^T[D_{hh}]\boldsymbol{V}_1 + \overline{\boldsymbol{\epsilon}}^T[D_{\epsilon\epsilon}]\overline{\boldsymbol{\epsilon}} + \boldsymbol{V}_0^T[D_{hh}]\boldsymbol{V}_0 + \boldsymbol{V}'^T_0[D_{ll}]\boldsymbol{V}_0' + 2\boldsymbol{V}_0^T[D_{h\epsilon}]\overline{\boldsymbol{\epsilon}} \\ &+ 2\boldsymbol{V}'^T_0[D_{l\epsilon}]\overline{\boldsymbol{\epsilon}} - 2\boldsymbol{V}_1^T[D_{l\epsilon}]\overline{\boldsymbol{\epsilon}}' + 2\boldsymbol{V}'^T_0[D_{hl}]\boldsymbol{V}_0 - 2\boldsymbol{V}'^T_0[D_{hl}]\boldsymbol{V}_1 + 2\boldsymbol{V}'^T_0[D_{hl}]\boldsymbol{V}_1)dx_1 \end{aligned} \tag{20}$$

The energy functional Equation (20) can be minimized to result in the Euler–Lagrange equation with the same procedure as Equation (15) so that $\left(\frac{\partial U_1}{\partial \boldsymbol{V}_1} = 0\right)$. we have

$$-[D_{hl}]^T\boldsymbol{V}_0' + [D_{hl}]\boldsymbol{V}_0' + [D_{hh}]\boldsymbol{V}_1 - [D_{l\epsilon}]^T\overline{\boldsymbol{\epsilon}}' = 0 \tag{21}$$

Using the Equations (21, 17), $\boldsymbol{V}_1$ can be calculated as

$$\boldsymbol{V}_1 = [D_{hh}]^{-1}[([D_{hl}]^T - [D_{hl}])[\widehat{V}_0] + [D_{l\epsilon}]^T]\overline{\boldsymbol{\epsilon}}' \equiv [\widehat{V}_1]\overline{\boldsymbol{\epsilon}}' \tag{22}$$

The strain energy functional Equation (19) can be obtained in terms of $\overline{\boldsymbol{\epsilon}}$, $\overline{\boldsymbol{\epsilon}}'$, and $\overline{\boldsymbol{\epsilon}}''$ by substituting Equation (17 and 22) to into Equation (19). We have

$$2U_1 = \int_L (\overline{\boldsymbol{\epsilon}}^T[A_1]\overline{\boldsymbol{\epsilon}} + \overline{\boldsymbol{\epsilon}}'^T[A_2]\overline{\boldsymbol{\epsilon}} + \overline{\boldsymbol{\epsilon}}'^T[A_3]\overline{\boldsymbol{\epsilon}}' + \overline{\boldsymbol{\epsilon}}^T[A_4]\overline{\boldsymbol{\epsilon}}'')dx_1 \tag{23}$$

In which the relations $[A_1]$, $[A_2]$, $[A_3]$, and $[A_4]$ are as follows.[10]

$$\begin{aligned}
[A_1] &= [D_{\epsilon\epsilon}] + 2[\widehat{V}_0]^T[D_{h\epsilon}] + [\widehat{V}_0][D_{hh}][\widehat{V}_0] \\
[A_2] &= 2[D_{l\epsilon}][\widehat{V}_0] + 2[\widehat{V}_0]^T[D_{hl}][\widehat{V}_0] \\
[A_3] &= 2[\widehat{V}_1]^T[D_{hl}][\widehat{V}_0] + [\widehat{V}_1]^T[D_{hh}][\widehat{V}_1] + [\widehat{V}_0]^T[D_{ll}][\widehat{V}_0] \\
[A_4] &= 2[\widehat{V}_0^T][D_{hl}][\widehat{V}_1] + 2[D_{l\epsilon}][\widehat{V}_1]
\end{aligned} \tag{24}$$

The use of Equation (23) includes derivatives of the 1D strains which is complicated. Therefore, in order to eliminate the derivatives of the 1D strains, the equilibrium equations are used to make a relationship between the strains and their derivatives. To do so, the transformation to the generalized Timoshenko theory is introduced in which the strain energy is converted to the generalized Timoshenko strain energy to take into account the shear strain effects. This procedure is carried out by deriving kinematic relations between asymptotically obtained 1D strains of Equation (4) and the generalized Timoshenko strains. The details of the procedure are expressed in References 3,7. It is noted that in the generalized Timoshenko beam model, the cross-section plane is not normal to the reference line in contrast to the classical beam model. The generalized Timoshenko strain energy is presented as

$$2U_1 = \int_L (\boldsymbol{\epsilon}^T[X]\boldsymbol{\epsilon} + 2\boldsymbol{\epsilon}^T[Y]\boldsymbol{\gamma}_s + \boldsymbol{\gamma}_s{}^T[G]\boldsymbol{\gamma}_s)dx_1 \tag{25}$$

In which $[X]$, $[Y]$ and $[G]$ are unknown stiffness matrices and $\boldsymbol{\gamma}_s = [2\gamma_{12}\ 2\gamma_{13}]^T$ includes generalized shear strains caused by the transverse shear deformation. $\boldsymbol{\epsilon} = \begin{bmatrix}\gamma_{11} & \kappa_1 & \kappa_2 & \kappa_3\end{bmatrix}^T$ contains the Timoshenko beam model generalized strains. The relation between $\boldsymbol{\epsilon}$ and $\overline{\boldsymbol{\epsilon}}$ is

$$\overline{\boldsymbol{\epsilon}} = \boldsymbol{\epsilon} + [P]\boldsymbol{\gamma}_s' \tag{26}$$

where

$$[P] = \begin{bmatrix} 0 & 0 & 0 & 1 \\ 0 & 0 & -1 & 0 \end{bmatrix}^T \tag{27}$$

The 1D linear equilibrium equations are employed as

$$\begin{aligned}
\boldsymbol{F}' &= 0 \\
\boldsymbol{M}' + [Q]\boldsymbol{F} &= 0
\end{aligned} \tag{28}$$

In which $\boldsymbol{F} = \begin{bmatrix}F_1 & F_2 & F_3\end{bmatrix}^T$ and $\boldsymbol{M} = \begin{bmatrix}M_1 & M_2 & M_3\end{bmatrix}^T$ are force and moment resultants. F_1 is the sectional axial force, F_2 and F_3 are sectional shear forces along x_2 and x_3, respectively. M_1 is the twist about x_1, M_2 and M_3 are sectional bending moments about x_2 and x_3, respectively. Besides, the matrix $[Q]$ is defined as

$$[Q] = \begin{bmatrix} 0 & 0 & 0 \\ 0 & 0 & -1 \\ 0 & 1 & 0 \end{bmatrix} \tag{29}$$

The relation between cross-sectional stress resultants and the 1D generalized strains can be written as

$$\begin{bmatrix} F_1 & M_1 & M_2 & M_3 & F_2 & F_3 \end{bmatrix}^T = \begin{bmatrix} [X] & [Y] \\ [Y]^T & [G] \end{bmatrix} \begin{Bmatrix} \boldsymbol{\epsilon} \\ \boldsymbol{\gamma}_s \end{Bmatrix} \tag{30}$$

Using the Equations (25, 26, 28, and 30), the derivatives of the 1D strains can be calculated in terms of $\boldsymbol{\epsilon}$ and $\boldsymbol{\gamma}_s$. The details of the procedure are explained in Hodges.[3] The unknown stiffness matrices $[X]$, $[Y]$, and $[G]$ can be expressed as follows.

$$\begin{aligned} [G] &= ([P]^T[A_1]^{-1}([A_3] - [A_2]^T[A_1]^{-1}[A_2])[A_1]^{-1}[P])^{-1} \\ [Y] &= [A_2]^T[A_1]^{-1}[P][G] \\ [X] &= [Y][G]^{-1}[Y]^T + [A_1] \end{aligned} \tag{31}$$

By calculating the stiffness matrices of Equation (31), one can rearrange the achieved stiffness constants to the form of strain energy of Equation (32) as follows.

$$2U_1 = \boldsymbol{\psi}^T[S]\boldsymbol{\psi} \tag{32}$$

In the strain energy of Equation (32) the effect of shear is considered where $\boldsymbol{\psi} = \begin{bmatrix} \gamma_{11} & 2\gamma_{12} & 2\gamma_{13} & \kappa_1 & \kappa_2 & \kappa_3 \end{bmatrix}^T$. Moreover, the matrix S contains the Timoshenko cross-sectional stiffness constants. S_{11} is the extensional stiffness, S_{22} and S_{33} are shear stiffness along x_2 and x_3, respectively and S_{44} is the torsional stiffness, S_{55} $(EI)_{x_2}$ and S_{66} $(EI)_{x_3}$ are bending stiffness about x_2 and x_3, respectively. The off-diagonal elements are coupling stiffness constants, that is, S_{14} is the extension-twist coupling and so on.

2.6 | One-dimensional finite element beam analysis

The strain energy Equation (32) which is applied for 1D beam analysis, includes 3D deformation effects of the cross-section. Therefore, the 1D static analysis of the tubular beam can be performed using this strain energy equation. The 1D strain energy of beam element is as follows

$$2U^e = \int_{L_e} \{\boldsymbol{\psi}^T[S]\boldsymbol{\psi}\} dx_1 \tag{33}$$

where $\boldsymbol{\psi} = \begin{bmatrix} \gamma_{11} & 2\gamma_{12} & 2\gamma_{13} & \kappa_1 & \kappa_2 & \kappa_3 \end{bmatrix}^T$ and L_e is the element length. We can calculate the stiffness of an element if we express the strains in Equation (33) in terms of degrees of freedom of beam element. For a Timoshenko beam model, we can use an element with three nodes which can prevent shear locking.[18] The element and its coordinate are shown in Figure 2. The element has 6 degrees of freedom at each node including three displacements ($\overline{u}$, $\overline{v}$, and $\overline{w}$) and three cross-sectional rotations ($\overline{\varphi}_{x_1}, \overline{\varphi}_{x_2}, \overline{\varphi}_{x_3}$) in the x_1, x_2, and x_3, respectively. Hence, 18 degrees of freedom for the element is considered. In this model, the following polynomials for the approximation of the degree of freedom in the length is used.[18]

$$\overline{u} = \overline{\alpha}_1 + \overline{\alpha}_2 x_1 + \overline{\alpha}_3 x_1^2 \tag{34a}$$

$$\overline{v} = \overline{\alpha}_4 + \overline{\alpha}_5 x_1 + \overline{\alpha}_6 x_1^2 + \overline{\alpha}_7 x_1^3 \tag{34b}$$

$$\overline{w} = \overline{\alpha}_8 + \overline{\alpha}_9 x_1 + \overline{\alpha}_{10} x_1^2 + \overline{\alpha}_{11} x_1^3 \tag{34c}$$

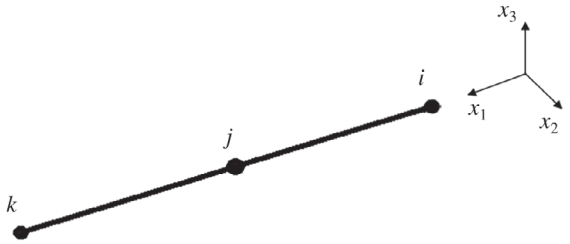

FIGURE 2 A beam element with three nodes[18]

$$\overline{\varphi}_{x_1} = \overline{\alpha}_{12} + \overline{\alpha}_{13}x_1 + \overline{\alpha}_{14}x_1^2 \tag{34d}$$

$$2\gamma_{12} = \overline{\alpha}_{15} + \overline{\alpha}_{16}x_1 \tag{34e}$$

$$2\gamma_{13} = \overline{\alpha}_{17} + \overline{\alpha}_{18}x_1 \tag{34f}$$

For a Timoshenko beam model, the 1D strains can be written as

$$\gamma_{11} = \overline{u'} \tag{35a}$$

$$\kappa_1 = \overline{\varphi'_{x_1}} \tag{35b}$$

$$\kappa_2 = \overline{\varphi'_{x_2}} \tag{35c}$$

$$\kappa_3 = \overline{\varphi'_{x_3}} \tag{35d}$$

$$2\gamma_{12} = \overline{v'} - \overline{\varphi}_{x_3} \tag{35e}$$

$$2\gamma_{13} = \overline{w'} + \overline{\varphi}_{x_2} \tag{35f}$$

It is noted that the $\overline{\varphi}_{x_2}$ and $\overline{\varphi}_{x_3}$ are the bending rotations of the beam section with respect to x_2 and x_3, respectively, while $2\gamma_{12}$ and $2\gamma_{13}$ are rotation of beam section about x_3 and x_2 for transverse shear deformation, respectively. Using strain–displacement Equation (35) and Equation (34), the rotations can be expressed as

$$\overline{\varphi}_{x_2} = \overline{\alpha}_{17} + \overline{\alpha}_{18}x_1 - \overline{\alpha}_9 - 2\overline{\alpha}_{10}x_1 - 3\overline{\alpha}_{11}x_1^2 \tag{36a}$$

$$\overline{\varphi}_{x_3} = -\overline{\alpha}_{15} - \overline{\alpha}_{16}x_1 + \overline{\alpha}_5 + 2\overline{\alpha}_6x_1 + 3\overline{\alpha}_7x_1^2 \tag{36b}$$

The column matrix of degrees of freedom of the beam element will be as follows

$$\begin{aligned}\boldsymbol{\delta} = [\,&\overline{u}^i \quad \overline{v}^i \quad \overline{w}^i \quad \overline{\varphi}^i_{x_1} \quad \overline{\varphi}^i_{x_2} \quad \overline{\varphi}^i_{x_3}\\ &\overline{u}^j \quad \overline{v}^j \quad \overline{w}^j \quad \overline{\varphi}^j_{x_1} \quad \overline{\varphi}^j_{x_2} \quad \overline{\varphi}^j_{x_3}\\ &\overline{u}^k \quad \overline{v}^k \quad \overline{w}^k \quad \overline{\varphi}^k_{x_1} \quad \overline{\varphi}^k_{x_2} \quad \overline{\varphi}^k_{x_3}\,]^T\end{aligned} \tag{37}$$

The unknown coefficients matrix is as the following

$$\overline{\boldsymbol{\alpha}} = [\overline{\alpha}_1 \;\; \overline{\alpha}_2 \;\; \ldots \;\; \overline{\alpha}_{18}] \tag{38}$$

The unknowns $(\overline{\alpha}_1 - \overline{\alpha}_{18})$ in the Equation (34) are expressed in terms of the nodal displacement vector $\boldsymbol{\delta}$ by substituting $\overline{u}, \overline{v}, \overline{w}, \overline{\varphi}_{x_1}, \overline{\varphi}_{x_2}$, and $\overline{\varphi}_{x_3}$ at all three nodes of the beam element. we have

$$\boldsymbol{\delta} = [T]\overline{\boldsymbol{\alpha}} \text{ or } \overline{\boldsymbol{\alpha}} = [T]^{-1}\boldsymbol{\delta} \tag{39}$$

The matrix $[T]$ has an order of 18×18 includes the element nodal coordinates. The 1D strain vector $\boldsymbol{\psi}$ can be expressed in terms of $\overline{\boldsymbol{\alpha}}$ using Equation (32) as

$$\boldsymbol{\psi} = [N]\overline{\boldsymbol{\alpha}} \tag{40}$$

where matrix $[N]$ has order of 6×18 which is a function of x_1. Finally, the strain vector $\boldsymbol{\psi}$ can be expressed in terms of nodal displacement vector $\boldsymbol{\delta}$ using Equation (40) as

$$\boldsymbol{\psi} = [N][T]^{-1}\boldsymbol{\delta} = [R]\boldsymbol{\delta} \tag{41}$$

The strain energy relation of the element can be written as

$$U^e = \frac{1}{2}\boldsymbol{\delta}^T \left\{ \int_{L_e} [R]^T[S][R]dx_1 \right\} \boldsymbol{\delta} \tag{42}$$

The stiffness matrix of the beam element is

$$[K^e] = \int_{L_e} [R^T][S][R]dx_1 \tag{43}$$

The nodal force vector caused by external loads and moments can be expressed as

$$\begin{aligned} \boldsymbol{f} = [f_1^i \quad f_2^i \quad f_3^i \quad m_1^i \quad m_2^i \quad m_3^i \\ f_1^j \quad f_2^j \quad f_3^j \quad m_1^j \quad m_2^j \quad m_3^j \\ f_1^k \quad f_2^k \quad f_3^k \quad m_1^k \quad m_2^k \quad m_3^k]^T \end{aligned} \tag{44}$$

where f is the vector of nodal force and f_1^i, f_1^j, f_1^k are extensional forces, f_2^i, f_2^j, f_2^k and f_3^i, f_3^j, f_3^k are transverse forces at nodes i, j, and k, and m_1^i, m_1^j, m_1^k are the torsional moments, $m_2^i m_2^j m_2^k$ and m_3^i, m_3^j, m_3^k are bending moments at nodes i, j, and k. The nodal displacement vector is achieved as follows.

$$\boldsymbol{\delta} = [K^e]^{-1}\boldsymbol{f} \tag{45}$$

2.7 | Step 8: Recovery analysis

The 3D strain distribution through the thickness of the tube can be obtained using Equations (2 and 26), and the use of $\boldsymbol{\epsilon}$ obtained from Equation (A2),.[3]

3 | DIMENSIONAL REDUCTION USING PASCAL POLYNOMIAL METHOD

3.1 | Novelty of the present work

In Equation (7), the warping functions are assumed to be a product of functions $W(x_2, x_3)$ and $V(x_1)$. There are sections of complex geometries such as beams with C section as shown in Figure 3. To handle these complex geometries, Yu et al.,[4] developed cross-sectional analysis of a composite box beams using VABS. The software performs FEA for cross-sectional discretization. It provides the equivalent stiffness for the section to be used in the subsequent 1D analysis (step 7) and recovery of the strains (step 8).

For composite beams of circular sections consisting of many layers such as that shown in Figure 4(A), the procedure to discretize the section using VABS is complex. The cross-section modeling procedure includes: (a) Defining two laminate sections as upper and lower laminate sections (the upside of the horizontal solid line is the upper laminate section and

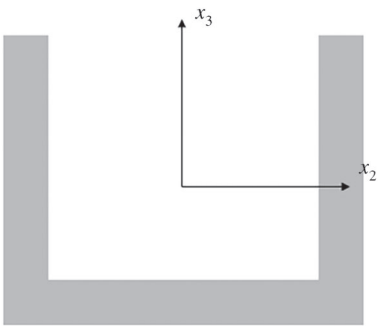

FIGURE 3 Beam of C section

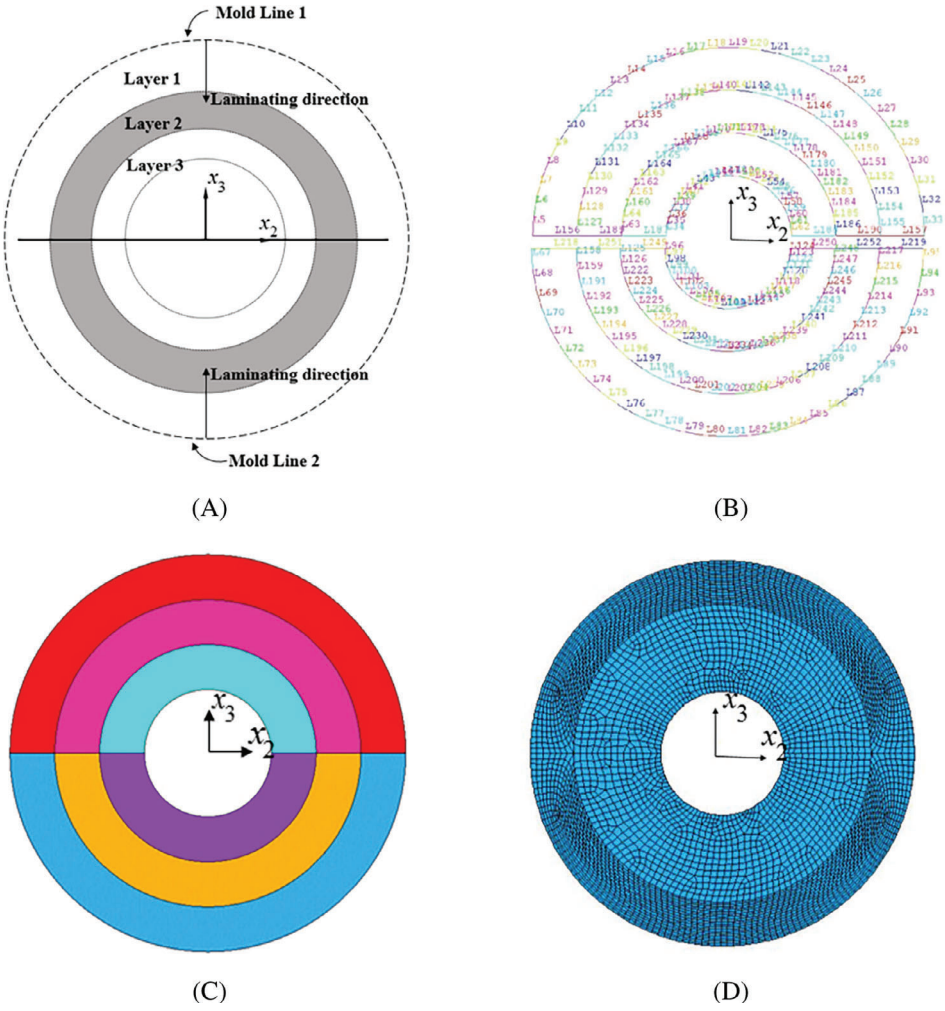

FIGURE 4 Discretization procedure in variational asymptotic beam sectional analysis. (A) Cross-sectional modeling of a tube; (B) segments of laminated section; (C) area of each layer; (D) the generated mesh of the cross section

downside is the lower laminate section) as shown in Figure 4(A), (B)) Decomposing each laminated section into segments and defining the lamination direction based on the defined mold lines (Figure 4(B)), (c) Generating areas of each layer (Figure 4(C)), (d) Meshing the areas over the cross-section using triangular or quadrilateral elements (Figure 4(D)).

The modeling process of the circular cross-section in the VABS is time-consuming, particularly for parametric study. This is also not necessary. The analysis of composite circular cross-section can be more straightforward and faster using polynomial based as shown below.

3.2 | Dimensional reduction using Pascal polynomial method

Note that in Equation (6), the first equality expresses the strain energy in terms of the 3D strains, and the second equality expresses the strain energy in terms of the warping functions w, its derivative with respect to the axis $x_1(\boldsymbol{w}')$, and the 1D strains of the reference line. For the analysis of composite tube, a cylindrical coordinate system is introduced. Figure 5(A) shows the beam Cartesian coordinates (x_1, x_2, and x_3), material coordinates (e_1, e_2, and e_3) where e_1 is along the fiber direction, and the beam reference line. The position of an arbitrary point in the cross-section is shown by a radial position r and a circumferential angle θ in the polar coordinate system. α represents the fiber orientation angle in its plane (winding angle). Figure 5(B) represents the cross-section of a single-layered tube with the inner and outer radius of r_{in} and r_{out}, respectively. The angle β denotes the layer orientation to axis x_2.

The matrix of stiffness coefficients $[C]$ within this local coordinate system is given by Equation (A3). A relation between $[C]$ and $[D]$ is required. This is done through two coordinate transformations. In the first transformation, the axis e_1 is rotated by an angle α to coincide with x_1. The transformation matrix $[T_\alpha]$ is given as Equation (A4). At the end of this rotation, the axes e_2, e_3 become e_2', e_3' and these may not coincide with the axes x_2, x_3. The angle β between the axis e_2' and x_2 which takes into account the orientation of the layer is used. A rotation of the axis e_2' by angle β to coincide with axis x_2 is done through a rotation matrix $[T_\beta]$ as shown in Equation (A5). As such one has

$$[D] = [T_\beta]^{-1}[T_\alpha]^{-1}[C][T_\alpha]^{-T}[T_\beta]^{-T}. \tag{46}$$

The relation between the circumferential angle and layer orientation can be introduced by a change of variable as $\beta = \theta - \frac{\pi}{2}$. In the discretization of warping field of Equation (7) used by VABS, the function $[W(x_2, x_3)]$ consists of FE shape functions, and the vector $\boldsymbol{V}$ is a column matrix of the nodal values of the warping displacement over the cross-section.[3] In the proposed Pascal polynomial approach, $w_k(x_1, x_2, x_3)$ is proposed to be a simple polynomial as

$$\begin{aligned} w_k(x_1, x_2, x_3) = {} & a_1 + a_2x_2 + a_3x_3 + a_4x_2^2 + a_5x_2x_3 + a_6x_3^2 + a_7x_2^3 + a_8x_2^2x_3 + a_9x_2x_3^2 + a_{10}x_3^3 \\ & + a_{11}x_2^4 + a_{12}x_2^3x_3 + a_{13}x_2^2x_3^2 + a_{14}x_2x_3^3 + a_{15}x_3^4, \end{aligned} \tag{47}$$

where $k = 1, 2, 3$. w_k can be expressed in the vector form as

$$w_k = \lfloor 1\ x_2\ \ldots\ x_2x_3^3\ \ x_3^4\ \rfloor.[a_1\ \ a_2\ \ldots\ a_{14}\ \ a_{15}]^{\mathrm{T}}. \tag{48}$$

The cross-sectional discretization in the polynomial method would be as follows.

$$w_k(x_1, x_2, x_3) = \boldsymbol{W_k}(x_2, x_3)\boldsymbol{V_k}(x_1), \tag{49}$$

where the vector $\boldsymbol{V}_k$ consists of unknown Pascal coefficients a_i which is a function of axial coordinate and should be determined. The Pascal polynomials as the warping functions are used for the whole section and the strain energy will be minimized with respect to a vector of coefficients $\boldsymbol{V_k}(x_1)$. It should be pointed out that in VABS which applies FE,

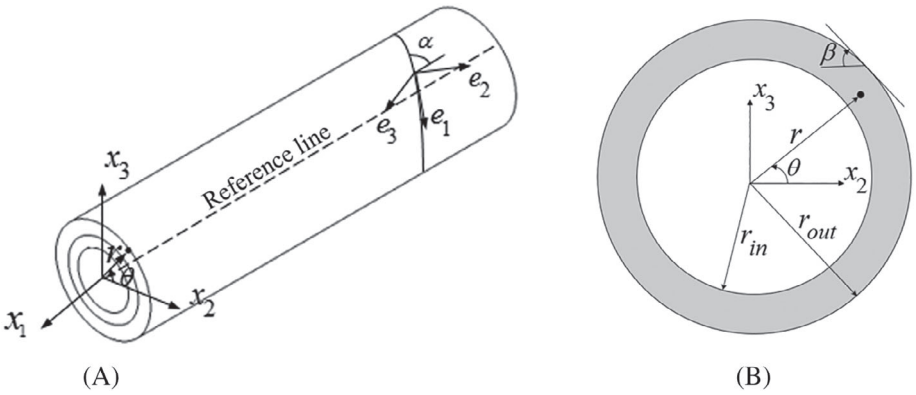

FIGURE 5 (A) Coordinate systems of a composite tubular beam, (B) The layer orientation of (β) in the circumference of a one-layer tube with inner and outer radius r_{in} and r_{out}

the warping at the common nodes at the interface between layers must set be to the same value, while in the Pascal polynomial method, the warping functions will be considered for the whole domain so that the problem of continuity of warping at the interfaces will be ensured. Using the polar coordinates, the transformation can be as ($x_2 = r\cos\theta$, $x_3 = r\sin\theta$). For polynomial with order m (i.e., $m = 4$), we have

$$\begin{aligned}\boldsymbol{W}_k = \; & [1 \quad r\cos(\theta) \quad r\sin(\theta) \quad r^2\cos^2(\theta) \quad r^2\cos(\theta)sin(\theta) \quad r^2\sin^2(\theta) \\ & r^3\cos^3(\theta) \quad r^3\cos(\theta)\sin^2(\theta) \quad r^3\cos^2(\theta)\sin(\theta) \quad r^3\sin^3(\theta) \quad r^4\cos^4(\theta) \\ & r^4\cos(\theta)\sin^3(\theta) \quad r^4\cos^3(\theta)\sin(\theta) \quad r^4\cos^2(\theta)\sin^2(\theta) \quad r^4\sin^4(\theta)],\end{aligned} \tag{50}$$

and,

$$V_k(x_1) = a(x_1). \tag{51}$$

The order of the polynomial can determine the accuracy of solution. A large number of layers will require higher polynomial order to assure accuracy. From Equation (4), $w = [w_1\ w_2\ w_3]^T$, the matrix form for the warping function is

$$\begin{Bmatrix} w_1 \\ w_2 \\ w_3 \end{Bmatrix} = \begin{bmatrix} [W_1]_{1\times p} & [O]_{1\times p} & [O]_{1\times p} \\ [O]_{1\times p} & [W_2]_{1\times p} & [O]_{1\times p} \\ [O]_{1\times p} & [O]_{1\times p} & [W_3]_{1\times p} \end{bmatrix}_{3\times q} . \begin{Bmatrix} V_1(x_1) \\ V_2(x_1) \\ V_3(x_1) \end{Bmatrix} \equiv [W].\boldsymbol{V}, \text{where } q = 3p, \tag{52}$$

where, p is the number of terms in the polynomial and $O_{1\times p}$ is a null matrix. The relation between the polynomial order m and the number of terms in the polynomial is $p = (m^2 + 3m + 2)/2$.

The integrations of $[D_{hh}]$, $[D_{h\epsilon}]$, $[D_{\epsilon\epsilon}]$, $[D_{hl}]$, $[D_{l\epsilon}]$, and $[D_{ll}]$ in the polynomial method for composite tube with n number of layers can be expressed as follows.

$$\begin{aligned}
[D_{hh}] &= \int_0^{2\pi}\int_{r_{in}}^{r_{out}} [\Gamma_h W]^T[D][\Gamma_h W] r dr d\theta = \sum_{i=1}^{n}\left(\iint_{\Omega_i} [\Gamma_h W]^T[D^i][\Gamma_h W] r dr d\theta\right) \\
[D_{h\epsilon}] &= \int_0^{2\pi}\int_{r_{in}}^{r_{out}} [\Gamma_h W]^T[D][\Gamma_\epsilon] r dr d\theta = \sum_{i=1}^{n}\left(\iint_{\Omega_i} [\Gamma_h W]^T[D^i][\Gamma_\epsilon] r dr d\theta\right) \\
[D_{\epsilon\epsilon}] &= \int_0^{2\pi}\int_{r_{in}}^{r_{out}} [\Gamma_\epsilon]^T[D][\Gamma_\epsilon] r dr d\theta = \sum_{i=1}^{n}\left(\iint_{\Omega_i} [\Gamma_\epsilon]^T[D^i][\Gamma_\epsilon] r dr d\theta\right) \\
[D_{hl}] &= \int_0^{2\pi}\int_{r_{in}}^{r_{out}} [\Gamma_h W]^T[D][\Gamma_l W] r dr d\theta = \sum_{i=1}^{n}\left(\iint_{\Omega_i} [\Gamma_h W]^T[D^i][\Gamma_l W] r dr d\theta\right) \\
[D_{ll}] &= \int_0^{2\pi}\int_{r_{in}}^{r_{out}} [\Gamma_l W]^T[D][\Gamma_l W] r dr d\theta = \sum_{i=1}^{n}\left(\iint_{\Omega_i} [\Gamma_l W]^T[D^i][\Gamma_l W] r dr d\theta\right) \\
[D_{l\epsilon}] &= \int_0^{2\pi}\int_{r_{in}}^{r_{out}} [\Gamma_l W]^T[D][\Gamma_\epsilon] r dr d\theta = \sum_{i=1}^{n}\left(\iint_{\Omega_i} [\Gamma_l W]^T[D^i][\Gamma_\epsilon] r dr d\theta\right),
\end{aligned} \tag{53}$$

where Ω_i is the area of the ith layer.

The use of VAM and VABS can greatly reduce the computational time and efforts for beams or tubes with complex cross-section.[4] For tubular composites with a large number of layers, the use of Pascal polynomial simplifies the input data and provides better insight into the problem. This is shown in the case studies below.

4 | VALIDATION OF THE RESULTS AND DISCUSSION

In order to validate the present method of solution, a program in Maple 15 has been developed named AMTSM (Analytical Meshless Tubular Sectional Method). To do so, various tubular sections with different lay-ups are utilized as case studies. The parametric study to investigate the effect of polynomial order and lay-up sequence on the accuracy of the method is presented.

4.1 | Validation of cross-sectional stiffness constants

4.1.1 | Aluminum tube

An aluminum 6061 T6[19] isotropic tubular section with the elastic modulus $E = 69.7$ GPa, Poisson ratio $\nu = 0.33$, an outer diameter $D_{\text{out}} = 88.9$ mm and the thickness $h = 3.175$ mm is studied. The obtained stiffness constants reported in Table 1 are compared with those extracted through the latest version of VABS as VABS 3.8 with the Classical beam model, and the Timoshenko beam model. The comparison between the proposed method and VABS 3.8 results Timoshenko and Classical are in terms of the stiffness constants which are obtained from 6×6 stiffness matrix (Timoshenko beam model) and 4×4 matrix (Classical beam model), respectively. As mentioned before, in the Timoshenko beam model, the effect of shear is considered while in the Classical beam model the effect of shear is not considered. It is noted that the present solution (Aluminum tube) has been done with ($m = 4$) of Pascal polynomials. On the other hand, the VABS 3.8 analysis is carried out with 6000 elements. It is observed that there is no difference in the obtained Timoshenko and Classical beam models in both methods of solutions.

4.1.2 | Composite tube with lay-up [20/ - 70/20/(-70)$_2$/20],[10]

As a second case study, a *thin* CUS composite tubular section is studied and the stiffness constants are compared with those in Reference 10 which used an earlier version of VABS, Reference 12, and VABS 3.8. The obtained results are tabulated in Table 2. The tube has lay-up sequence $[20/-70/20/-70_2/20]$ as shown in Figure 6. It has inner diameter $D_{\text{in}} = 1.934$ *in* (49.12 mm) and outer diameter $D_{\text{out}} = 2$ inches (50.8 mm) with the thickness of each layer of 0.0055 inches (0.1397 mm). It is made of IM6/R6376 with the material properties as $E_{11} = 23.1 \times 10^6$ psi (159.268 GPa), $E_{22} = 1.4 \times 10^6$ psi (9.652 GPa), $\nu_{12} = 0.338$ and $G_{12} = 0.73 \times 10^6$ psi (5.033 GPa). The stiffness constants based on the Timoshenko beam model (proposed method) agree well with Rehfield et al.[12] There are errors in the VABS (Timoshenko) results obtained by Popescu and Hodges[10] with respect to both present (Timoshenko) and Rehfield et al.[12] This error was modified in the higher versions of VABS proposed by Yu et al.[4] To this end, we analyzed this tube using VABS 3.8 with 7588 elements and the obtained results are reported. It can be seen that there is a large difference in the obtained stiffness constants between Timoshenko solution and Classical Solution, which can be due to the higher-order approximation of energy in Timoshenko and considering the shear effect. There is a sign difference in the calculated S_{14} and S_{36} of Rehfield et al.[12] and the results of Reference 10

TABLE 1 The nonzero cross-sectional stiffness constants of an aluminum tube

(Nonzero stiffness constants)	Present (Classical beam model)	Present (Timoshenko beam model)	VABS 3.8 (Classical beam model)	VABS 3.8 (Timoshenko beam model)	Strength of materials
S_{11} (N)	5.891×10^7	5.891×10^7	5.959×10^7	5.959×10^7	5.959×10^7
S_{22} (N)	—	1.140×10^7	—	1.122×10^7	—
S_{33} (N)	—	1.140×10^7	—	1.122×10^7	—
S_{44} (N.m^2)	4.168×10^4	4.168×10^4	4.121×10^4	4.121×10^4	4.217×10^4
S_{55} (N.m^2)	5.419×10^4	5.419×10^4	5.482×10^4	5.482×10^4	5.482×10^4
S_{66} (N.m^2)	5.419×10^4	5.419×10^4	5.482×10^4	5.482×10^4	5.482×10^4

Abbreviation: VABS, Variational Asymptotic Beam Sectional Analysis.

TABLE 2 Stiffness constants of circumferentially uniform stiffness tube, [20/ - 70/20/ - 70_2/20]

(Nonzero stiffness constants)	Beam theory	$S_{11} \times 10^6$ (lb)	S_{22} ($\times 10^5$) (lb)	S_{33} ($\times 10^5$) (lb)	S_{14} ($\times 10^5$) (lb.in)	S_{25} ($\times 10^6$) (lb.in)	S_{36} ($\times 10^6$) (lb.in)	S_{44} ($\times 10^5$) ($lb.in^2$)	S_{55} ($\times 10^5$) ($lb.in^2$)	S_{66} ($\times 10^5$) ($lb.in^2$)
$m = 3$	(Cl.)	1.938	—	—	−6.452	—	—	4.408	4.902	4.902
	(Tim.)	1.938	2.333	2.333	−6.452	3.226	3.226	4.408	9.364	9.364
$m = 4$	(Cl.)	1.938	—	—	−6.452	—	—	4.408	4.799	4.799
	(Tim.)	1.938	2.333	2.333	−6.452	3.226	3.226	4.408	9.364	9.364
$m = 5$	(Cl.)	1.938	—	—	−6.452	—	—	4.407	4.799	4.799
	(Tim.)	1.938	2.280	2.280	−6.452	3.226	3.226	4.407	9.364	9.364
$m = 7$	(Cl.)	1.938	—	—	−6.452	—	—	4.407	4.798	4.798
	(Tim.)	1.938	2.279	2.279	−6.452	3.226	3.226	4.407	9.363	9.363
VABS 3.8	(Cl.)	1.896	—	—	−6.249	—	—	4.386	4.798	4.901
	(Tim.)	1.896	2.276	2.259	−6.161	3.220	3.028	4.386	9.354	8.959
Rehfield et al.[12]	Non-Cl.	1.972	2.317	2.317	6.680	−3.340	4.634	4.159	9.862	9.862
Popescu and Hodges[10]	(Cl.)	1.886	—	—	6.086	—	—	4.159	4.831	4.831
Popescu and Hodges[10]	(Tim.)	1.886	1.137	1.137	6.086	−1.609	−1.609	4.159	7.109	7.109

Abbreviation: VABS, Variational Asymptotic Beam Sectional Analysis.

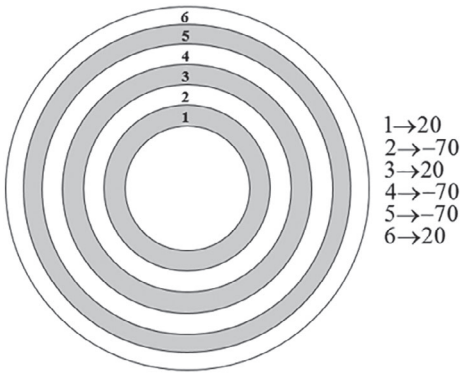

FIGURE 6 Cross-section with lay up of [20/ - 70/20/ - 70_2/20]

which can be a result of sign convention in each of the works. Moreover, the stiffness constants of the tube are computed with different orders of the polynomial ($m = 3$ and 4). The obtained stiffness constants are converged by $m = 4$.

4.1.3 | A thick composite tube with lay-up [$90_{30}/\pm25_{45}/90_5/\pm30_{20}/90_5/\pm45_{20}$]

The third case study is related to a thick composite tube with complicated lay-up sequence [$90_{30}/\pm25_{45}/90_5/\pm30_{20}/90_5/\pm45_{20}$]. The tube is fabricated using Automated Fiber Placement (AFP) technique with material of Carbon/PEKK with $E_1 = 138.3$ GPa, $E_2 = E_3 = 10.1$ GPa, $\nu_{12} = \nu_{13} = 0.31$, $\nu_{23} = 0.33$ and $G_{12} = G_{13} = G_{23} = 5.56$ GPa. The tube has inner and outer diameters $D_{\text{in}} = 56$ mm and $D_{\text{out}} = 98$ mm, respectively. The tube cross-section is meshed using VABS 3.8 with 9098 elements as shown in Figure 7. The obtained stiffness constants are reported in Table 3. There is a large difference in the obtained flexural stiffness (S_{55} and S_{66}) between Cl. and Timosheko models. In addition, the obtained stiffness constants are compared with those of the 3D elasticity solution of Lekhnitskii for multilayered composite tubes proposed by Jolicoeur and Cardou[20] and Moshir et al.[21] with no-slip assumption at the interfaces of the layers as well as Shadmehri et al.[22] who used nonclassical beam theory to calculate flexural stiffness of composite tube. A good agreement between the obtained stiffness constants and the literature is observed.

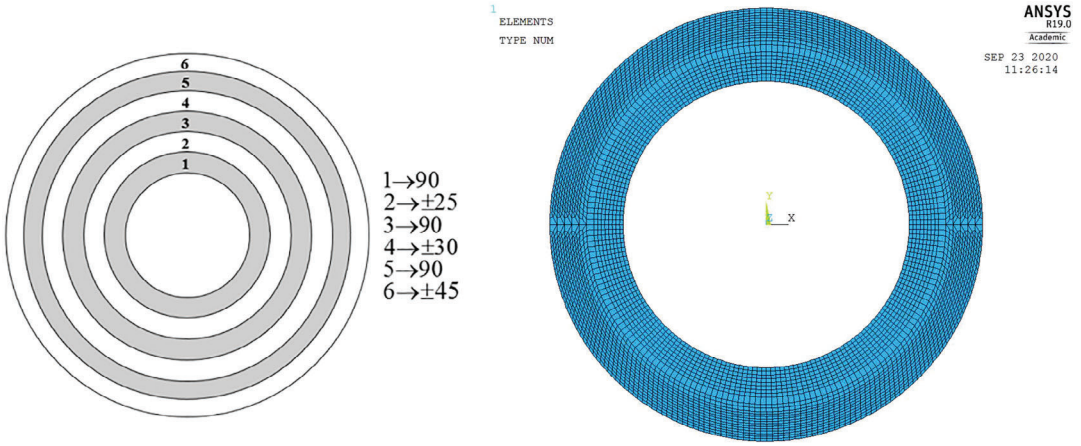

FIGURE 7 (A) The lay-up sequence, (B) generated mesh of the composite tube with 9098 number of elements

TABLE 3 Nonzero stiffness constants for tube $[90_{30}/\pm25_{45}/90_5/\pm30_{20}/90_5/\pm45_{20}]$

(Nonzero stiffness constants)	Beam theory	S_{11} ($\times 10^8$) (N)	S_{22} ($\times 10^7$) (N)	S_{33} ($\times 10^7$) (N)	S_{14} ($\times 10^6$) (N.m)	S_{25} ($\times 10^6$) (N.m)	S_{36} ($\times 10^6$) (N.m)	S_{44} ($\times 10^5$) ($N.m^2$)	S_{55} ($\times 10^5$) ($N.m^2$)	S_{66} ($\times 10^5$) ($N.m^2$)
$m = 4$	(Cl.)	2.955	—	—	−5.088	—	—	1.795	1.035	1.035
	(Tim.)	2.955	5.073	5.073	−5.088	2.408	5.073	1.795	2.178	2.178
$m = 5$	(Cl.)	2.953	—	—	−5.087	—	—	1.795	1.017	1.031
	(Tim.)	2.953	5.008	5.010	−5.087	2.407	2.378	1.795	2.175	2.160
$m = 7$	(Cl.)	2.953	—	—	−5.087	—	—	1.795	1.017	1.017
	(Tim.)	2.953	5.008	5.010	−5.087	2.407	2.378	1.795	2.175	2.160
VABS 3.8	(Cl.)	2.945	—	—	−5.071	—	—	1.787	0.993	0.994
	(Tim.)	2.945	4.786	4.786	−5.071	2.328	2.326	1.787	2.126	2.125
Shadmehri et al.[22]	Non-Cl.	—	—	—	—	—	—	—	2.228	2.228
Jolicoeur and Cardou[20]	3D elasticity	—	—	—	—	—	—	—	2.162	2.162

Abbreviation: VABS, Variational Asymptotic Beam Sectional Analysis.

4.2 | Effect of polynomial order (m), and lay-up sequence, on the accuracy of the stiffness constants of the cross-section

The selected order of Pascal polynomial in the warping field, and lay-up sequence may affect the accuracy of not only the stiffness constants of the tube but also on the 3D strains of the tube. To this end, we examined composite tubes with material properties $E_1 = 140$ GPa, $E_2 = E_3 = 10$ GPa, $\nu_{12} = \nu_{13} = 0.31$, $\nu_{23} = 0.33$ and $G_{12} = G_{13} = G_{23} = 5.53$ GPa. The outer and inner radiuses of the tubes are $r_{out} = 59$ mm and $r_{out} = 39$ mm, respectively. The thickness of each layer is assumed to be 2 mm. Note that all the following reported stiffness constants are in SI.

4.2.1 | Unidirectional composite tube $[0_{10}]$

The effect of polynomial order on the accuracy of stiffness constants of a unidirectional tube is investigated in Table 4. Values are compared with those obtained from VABS 3.8. Except for S_{22} of ($m = 2$), the other stiffness constants are close to which obtained by VABS 3.8. The obtained S_{22} and S_{33} of orders ($m = 5$ and 7) are more accurate compared to other orders. It is noted that both the obtained Timoshenko and Classical are the same.

TABLE 4 Stiffness constants for tube $[0_{10}]$, $r_{out} = 0.059$ m, ply thickness $t = 2$ mm, for both (Cl. and Tim.)

(Nonzero stiffness constants)	S_{11} ($\times 10^8$)	S_{22} ($\times 10^7$)	S_{33} ($\times 10^7$)	S_{44} ($\times 10^4$)	S_{55} ($\times 10^6$)	S_{66} ($\times 10^6$)
$m = 2$	8.620	3.404	3.404	8.516	1.077	1.077
Diff.%	0	87.130	87.130	0	0	0
$m = 3$	8.620	1.983	1.983	8.516	1.077	1.077
Diff.%	0	9.015	9.015	0	0	0
$m = 4$	8.620	1.983	1.983	8.516	1.077	1.077
Diff.%	0	9.015	9.015	0	0	0
$m = 5$	8.620	1.890	1.890	8.516	1.077	1.077
Diff.%	0	3.903	3.903	0	0	0
$m = 7$	8.620	1.890	1.890	8.516	1.077	1.077
Diff.%	0	3.903	3.903	0	0	0
VABS 3.8	8.620	1.819	1.819	8.516	1.077	1.077
Strength of mat.	8.620	—	—	8.516	1.077	1.077

Abbreviation: VABS, Variational Asymptotic Beam Sectional Analysis.

TABLE 5 Stiffness constants for tube $[90_5/0_5]$, $r_{out} = 0.059$ m, ply thickness $t = 2$ mm, for both (Cl. and Tim.) theories

(Nonzero stiffness constants)	S_{11} ($\times 10^8$)	S_{22} ($\times 10^7$)	S_{33} ($\times 10^7$)	S_{44} ($\times 10^4$)	S_{55} ($\times 10^5$)	S_{66} ($\times 10^5$)
$m = 2$	5.104	3.405	3.405	8.516	7.315	7.315
Diff.%	1.189	65.935	65.935	0	0.480	0.480
$m = 3$	5.047	2.207	2.207	8.516	7.315	7.315
Diff.%	0.059	7.553	7.553	0	0.480	0.480
$m = 4$	5.047	2.207	2.207	8.516	7.281	7.281
Diff.%	0.059	7.553	7.553	0	0.480	0.013
$m = 5$	5.047	2.131	2.189	8.516	7.281	7.281
Diff.%	0.059	6.676	6.676	0	0.480	0.013
$m = 7$	5.045	2.131	2.189	8.516	7.281	7.281
Diff.%	0.029	6.676	6.676	0	0.480	0.013
VABS 3.8	5.044	2.052	2.052	8.516	7.280	7.280
Strength of mat.	5.026	—	—	8.516	7.256	7.256

Abbreviation: VABS, Variational Asymptotic Beam Sectional Analysis.

4.2.2 | Composite tubes with lay-up $[90_5/0_5]$

The effect of polynomial order (m) on the accuracy of the obtained flexural stiffness of cross-ply tube $[90_5/0_5]$, is demonstrated in Table 5. It is observed that the obtained Classical and Timoshenko flexural stiffness of the tube are similar when polynomial order increases. Increasing the polynomial order from 4 to 7 does not have a significant effect on the accuracy of the predicted flexural stiffness for tubes. Also, both the Timoshenko and Classical common stiffness constants are the same. The obtained results converge for $[90_5/0_5]$ with order ($m = 7$) of the polynomial.

4.2.3 | Composite tubes with lay-up $[\pm 60_5]$

The influence of polynomial order on the nonzero stiffness constants of the tube $[\pm 60_5]$ is investigated, as shown in Table 6. It is observed that for order ($m = 2$) of the polynomial, except for S_{14}, there is no significant difference

TABLE 6 Stiffness constants for tube $[\pm 60_5]$, $r_{out} = 59$ mm, ply thickness $t = 2$ mm, for both (Cl. and Tim.)

(Nonzero stiffness constants)	Beam theory	S_{11} ($\times 10^7$)	S_{22} ($\times 10^7$)	S_{33} ($\times 10^7$)	S_{14} ($\times 10^4$)	S_{25} ($\times 10^4$)	S_{36} ($\times 10^5$)	S_{44} ($\times 10^5$)	S_{55} ($\times 10^4$)	S_{66} ($\times 10^4$)
$m = 2$	(Cl.)	7.281	—	—	−3.340	—	—	4.395	9.085	9.085
	Diff%	0.289	—	—	25.346	—	—	0.365	0.0771	0.0771
	(Tim.)	7.281	9.410	9.410	−3.340	2.226	2.226	4.395	9.085	9.085
	Diff%	0.289	4.416	4.416	25.346	14.318	14.351	0.365	0.066	0.066
$m = 3$	(Cl.)	7.261	—	—	−4.351	—	—	4.390	9.084	9.084
	Diff%	0.013	—	—	2.749	—	—	0.251	0.055	0.055
	(Tim.)	7.261	9.118	9.118	−4.351	2.094	2.094	4.390	9.085	9.085
	Diff%	0.013	1.176	1.176	2.749	19.399	19.399	0.251	0.066	0.066
$m = 4$	(Cl.)	7.261	—	—	−4.351	—	—	4.390	9.075	9.075
	Diff%	0.013	—	—	2.749	—	—	0.251	0.033	0.033
	(Tim.)	7.261	9.128	9.128	−4.351	2.565	2.565	4.390	9.076	9.076
	Diff%	0.013	1.287	1.287	2.749	1.270	1.270	0.251	0.044	0.033
$m = 5$	(Cl.)	7.260	—	—	−4.383	—	—	4.389	9.075	9.075
	Diff%	0.000	—	—	2.033	—	—	0.228	0.033	0.033
	(Tim.)	7.260	9.106	9.124	−4.383	2.552	2.567	4.389	9.076	9.076
	Diff%	0.000	1.043	1.242	2.033	1.770	1.231	0.228	0.033	0.033
$m = 7$	(Cl.)	7.263	—	—	−4.844	—	—	4.390	9.077	9.077
	Diff%	0.0413	—	—	8.270	—	—	0.251	0.011	0.011
	(Tim.)	7.263	9.108	9.125	−4.844	2.749	2.762	4.390	9.078	9.078
	Diff%	0.0413	1.065	1.253	8.270	5.812	6.271	0.251	0.011	0.011
VABS 3.8	(Cl.)	7.260	—	—	−4.474	—	—	4.379	9.078	9.078
	(Tim.)	7.260	9.012	9.012	−4.474	2.598	2.599	4.379	9.079	9.079

Abbreviation: VABS, Variational Asymptotic Beam Sectional Analysis.

between the obtained (Cl.) results and those obtained by VABS 3.8. By increasing the order of the polynomial, the values of S_{14} become close to VABS 3.8. The two stiffness constants S_{22} and S_{33} of the order ($m = 2$) have a large difference compared with VABS 3.8. As the polynomial order increases, the difference decreases noticeably. A very good agreement between the results of the present approach with ($m = 7$) compared to VABS 3.8 is observed. In addition, it can be observed that the Classical and Timoshenko stiffness constants for this type of lay-up sequence $[\pm\alpha_5]$ are the same.

4.2.4 | Composite tubes with lay-up $[45_5/15_5]$

To further investigate the effect of lay-up sequence on the accuracy of the present approach, we evaluate flexural stiffness of angle-ply $[45_5/15_5]$ tube. Table 7 shows the effect of polynomial order on the stiffness of tubes $[45_5/15_5]$. Also, it is seen that increasing Pascal polynomial order, increases the accuracy of stiffness prediction.

There is a large difference between the obtained flexural stiffness (S_{55} and S_{66}) of the Classical and Timoshenko for both the methods. Which means that combination of angle-ply layers causes difference between the Classical and Timoshenko results. This difference between Classical and Timoshenko is due to the effect of shear strains which are considered in Timoshenko beam model. It is observed that the other common stiffness constants of the Classical and Timoshenko are the same. The percentage difference of the $m = 2$ values compared to VABS 3.8 is large. By increasing the polynomial order to ($m = 5$ or 7), the percentage difference decreases. The maximum of the percentage difference between the present results and VABS 3.8 is 7.690 for $S_{22,}$ whereas the minimum of the percentage difference is 0.485 for flexural stiffness (S_{66}).

4.3 | Validation of 3D strains

4.3.1 | Distribution of strain in tube $[90_{40}/25_{40}/90_{20}/30_{40}/90_{20}/45_{40}]$

To study the capability of the present method to predict strain distribution in the cross-section, the distribution of the 3D strain components in a composite cross-section with a complex lay-up $[90_{40}/25_{40}/90_{20}/30_{40}/90_{20}/45_{40}]$, the material properties of the Section 5.2., the length of 1 m, outer radius $r_{\text{out}} = 59$ mm, inner radius $r_{\text{in}} = 39$ mm and thickness of each layer 0.1 mm subjected to a pure bending moment $M_2 = 1$ KN.m are illustrated in Figures 8 to 11, respectively. The distribution variation and magnitude of Γ_{11}, $2\Gamma_{12}$, Γ_{22}, and Γ_{33} of the present method with $m = 7$ have a good correlation with respect to ANSYS 3D. The distribution of the normal strains through the thickness at $\theta = 90°$ of the circumference are demonstrated in Figure 12. The obtained results of the present method are compared with ANSYS 3D FE solution. In the ANSYS 3D solution, the element SOLID 185 has been used. The tube body is meshed with 3192 k elements. The total computational time of ANSYS 3D solution is 55 min while the present polynomial method computational time is only 15 s.

4.3.2 | Distribution of 3D strains of $[\pm 60_5]$ tube

The distribution of longitudinal strain Γ_{11}, Γ_{22} (normal strain along x_2), Γ_{33} (normal strain along x_3) and out-of-plane shear strain Γ_{12} through the thickness at $\theta = \frac{\pi}{2}$ of the tube $[\pm 60_5]$ with the material properties and dimensions of the Section 5.2 under $M_2 = 1$ KN.m are demonstrated in Figure 13. The order ($m = 7$) of the polynomial is used for the analysis. An excellent correlation between the present method and VABS 3.8 can be observed. It is noted that the tube is meshed with 97,800 elements in ANSYS 3D and the cross-section is meshed with 3740 2D elements in VABS 3.8.

4.4 | Validation of present 1D FE analysis

The deflection of the tubular composite beam calculated using the present polynomial (Section 4) and 1D FE (Section 3.6) is compared with VABS 3.8 and experimental result. For the experiment, we carried out a test on a composite tube under four points bending loading. The tube was made using an AFP machine. The wall thickness of the tube consists of two parts. The first inner part consists of seven layers of Carbon/Epoxy five-harness satin woven which the fibers are

TABLE 7 Stiffness constants for tube $[45_5/15_5]$, $r_{out} = 59$ mm, ply thickness $t = 2$ mm, (Cl. and Tim)

(Nonzero stiffness constants)	Beam theory	S_{11} ($\times 10^8$)	S_{22} ($\times 10^7$)	S_{33} ($\times 10^7$)	S_{14} ($\times 10^6$)	S_{25} ($\times 10^6$)	S_{36} ($\times 10^6$)	S_{44} ($\times 10^5$)	S_{55} ($\times 10^5$)	S_{66} ($\times 10^5$)
$m = 2$	(Cl.)	4.615	—	—	−6.805	—	—	2.533	4.884	4.884
	Diff%	3.847	—	—	17.024	—	—	29.300	7.152	7.152
	(Tim.)	4.615	7.482	7.482	−6.805	3.603	3.603	2.533	6.619	6.619
	Diff%	3.847	42.081	42.081	17.024	16.038	16.038	29.300	3.599	3.599
$m = 3$	(Cl.)	4.479	—	—	−6.004	—	—	2.060	4.692	4.692
	Diff%	0.078	—	—	3.250	—	—	5.155	2.939	2.939
	(Tim.)	4.479	6.833	6.833	−6.004	3.532	3.532	2.060	6.518	6.518
	Diff%	0.078	29.756	29.756	3.250	13.752	13.752	5.155	2.019	2.019
$m = 4$	(Cl.)	4.479	—	—	−6.004	—	—	2.060	4.620	4.620
	Diff%	0.078	—	—	3.250	—	—	5.155	1.360	1.360
	(Tim.)	4.479	5.690	5.690	−6.004	3.203	3.203	2.060	6.424	6.424
	Diff%	0.078	8.051	8.051	3.250	3.156	3.156	5.155	0.547	0.547
$m = 5$	(Cl.)	4.468	—	—	−5.939	—	—	2.023	4.613	4.619
	Diff%	0.540	—	—	2.132	—	—	3.266	1.206	1.338
	(Tim.)	4.468	5.678	5.675	−5.939	3.205	3.197	2.023	6.423	6.420
	Diff%	0.540	7.823	7.766	2.132	3.220	2.962	3.266	0.532	0.485
$m = 7$	(Cl.)	4.468	—	—	−5.939	—	—	2.023	4.613	4.617
	Diff%	0.540	—	—	2.132	—	—	3.266	1.206	1.338
	(Tim.)	4.468	5.671	5.662	−5.939	3.203	3.194	2.023	6.422	6.420
	Diff%	0.540	7.690	7.519	2.132	3.156	2.866	3.266	0.532	0.485
VABS 3.8	(Cl.)	4.444	—	—	−5.815	—	—	1.959	4.558	4.558
	(Tim.)	4.444	5.266	5.266	−5.815	3.105	3.105	1.959	6.389	6.389

Abbreviation: VABS, Variational Asymptotic Beam Sectional Analysis.

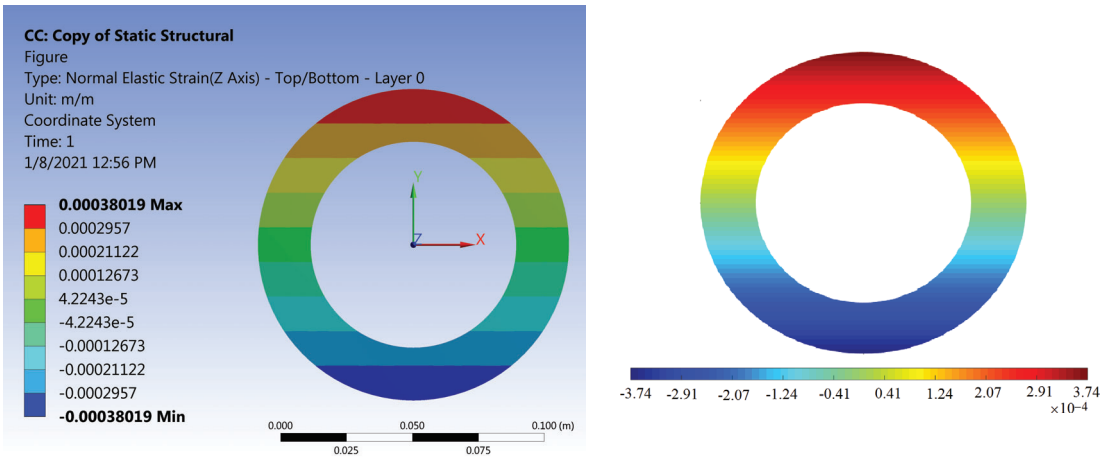

(A) ANSYS 3-D (B) Present

FIGURE 8 Distribution of Γ_{11} in the tubular section $[90_{40}/25_{40}/90_{20}/30_{40}/90_{20}/45_{40}]$ under ($M_2 = 1$ KN.m), (A) ANSYS 3D, (B) present

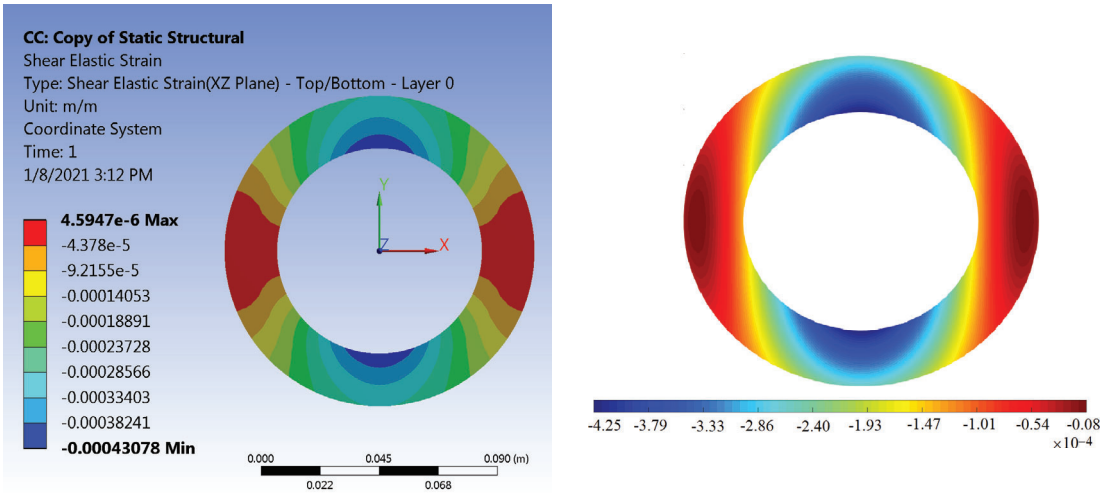

(A) ANSYS 3-D (B) Present

FIGURE 9 Distribution of $2\Gamma_{12}$ in the section $[90_{40}/25_{40}/90_{20}/30_{40}/90_{20}/45_{40}]$ under ($M_2 = 1$ KN.m), (A) ANSYS 3D, (B) present

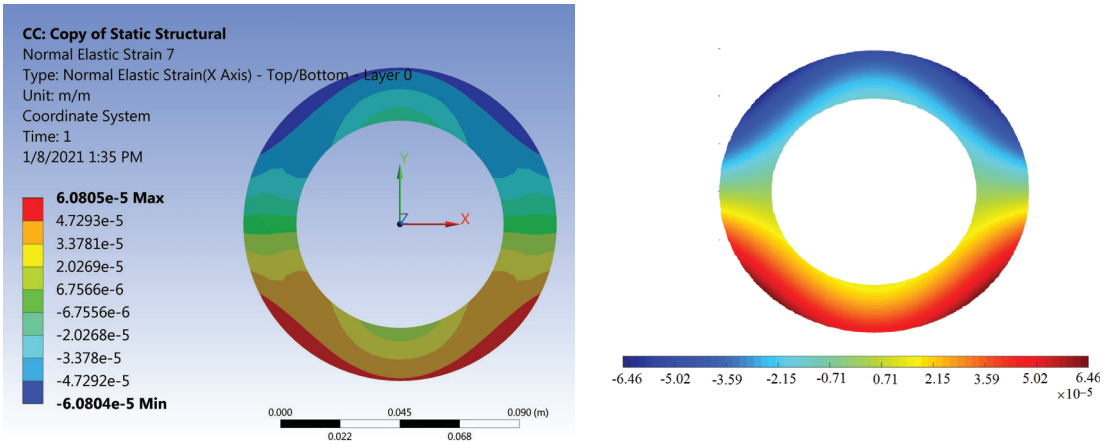

(A) ANSYS 3-D (B) Present

FIGURE 10 Distribution of Γ_{22} in the section $[90_{40}/25_{40}/90_{20}/30_{40}/90_{20}/45_{40}]$ under ($M_2 = 1$ KN.m), (A) ANSYS 3D, (B) present

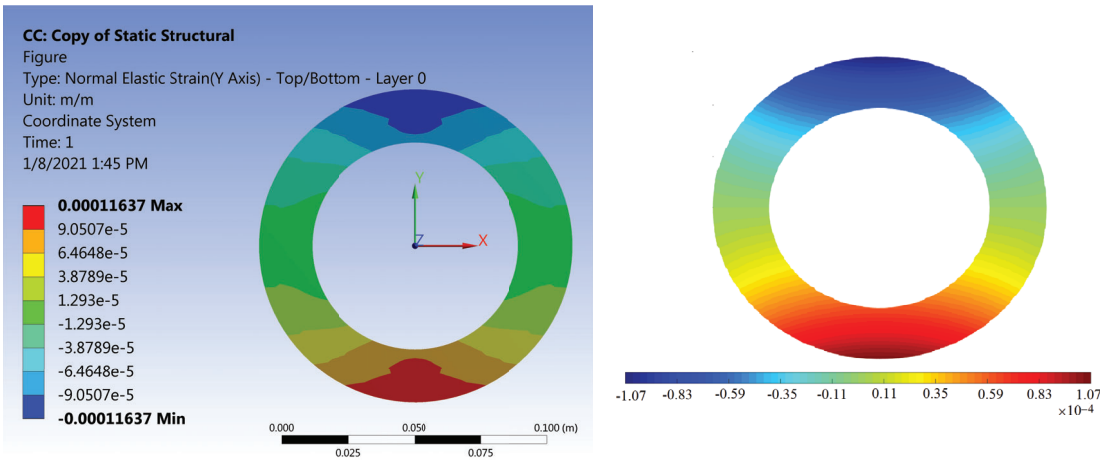

(A) ANSYS 3-D (B) Present

FIGURE 11 Distribution of Γ_{33} in the section $[90_{40}/25_{40}/90_{20}/30_{40}/90_{20}/45_{40}]$ under ($M_2 = 1$ KN.m), A) ANSYS 3D, B) present

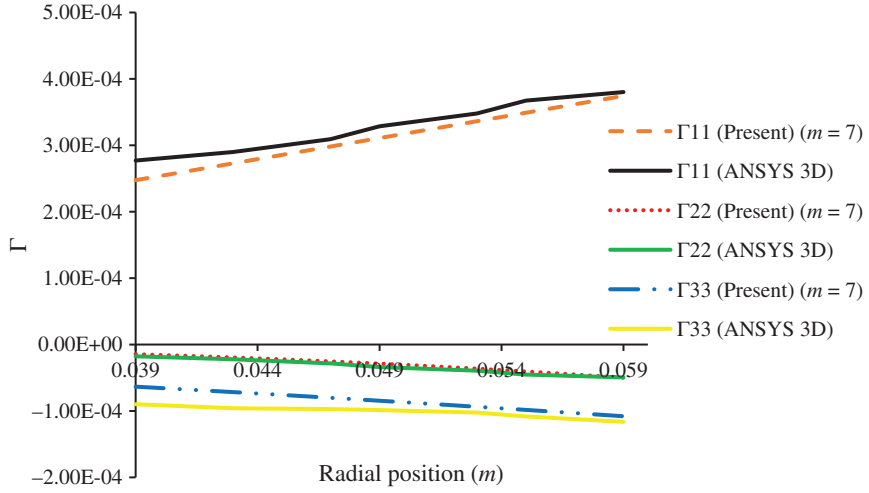

FIGURE 12 Distribution of Γ_{11}, Γ_{22}, and Γ_{33} through the thickness of $[90_{40}/25_{40}/90_{20}/30_{40}/90_{20}/45_{40}]$tube at $\theta = 90^o$ of the circumference under $M_2 = 1$ KN.m

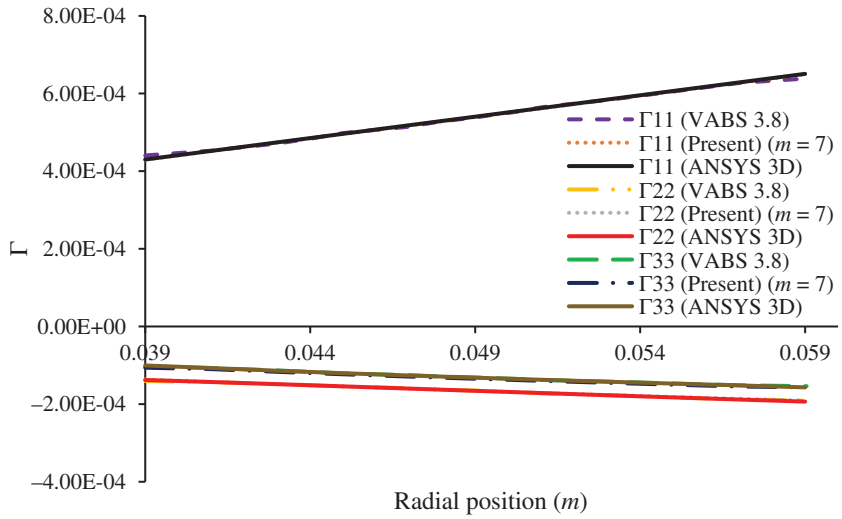

FIGURE 13 Distribution of Γ_{11}, Γ_{22}, and Γ_{33} through the thickness of $[\pm 60_5]$ tube at $\theta = 90^o$ of the circumference under $M_2 = 1$ KN.m

parallel and perpendicular to the axis of the tube. The second part consists of layers of Carbon/PEEK with the lay-up sequence $[90_4/(\pm 25)_4/90_4/(\pm 35)_4/90_4/(\pm 45)_4]$. The details of experimental test setup, tube dimensions, material property and etc. were reported in Reference 21. The tube was under the load 10 KN. The obtained VABS 3.8 stiffness matrix was imported to ANSYS APDL package to perform 1D FE analysis. In the ANSYS modeling, beam 189 element type was selected which has three nodes and 3 degrees of freedom at each node. The boundary conditions are considered as $(\overline{u} = \overline{v} = \overline{w} = 0, \overline{\varphi}_{x_1} = \overline{\varphi}_{x_3} = 0)$ at two ends of the beam. The distribution of transverse displacement in the length of the tube is demonstrated in Figure 14, with the experimental point at mid length of the tube. The convergence study shows that the obtained displacement converges with 40 number of 1D elements. It can be seen that a good agreement is obtained.

4.5 | Parametric study

In Figures 15–17, we investigated the influence of the fiber angle α on the change of stiffness constants S_{11}, S_{14}, S_{36}, S_{33}, S_{55}, and S_{66} of the composite tubes with lay-up $[\pm\alpha_5]$. The dimensions and material properties are similar to Section 5.2. It is seen from Figure 15 that as the fiber angle increases, the extensional stiffness (S_{11}) decreases. The change of S_{11} is considerable until the fiber angle of $\alpha = 45°$. The change of extensional-torsional (S_{14}) and torsional-bending (S_{36}) stiffness versus the fiber angle are depicted in Figure 16. At the fiber angle $\alpha = 30°$, the maximum of the S_{14} and S_{36} can be observed. Then, the value of them decrease considerably by $\alpha = 60°$. The variation of torsional and bending stiffness in

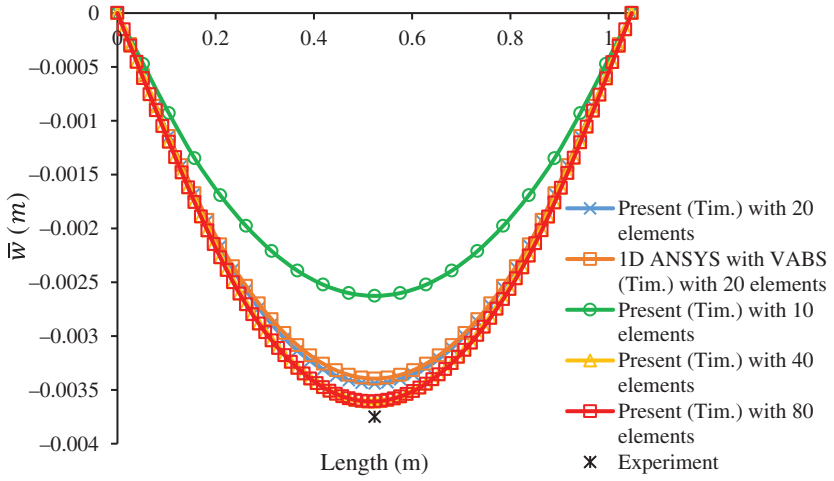

FIGURE 14 Transverse displacement of tube $[(5\text{Harness satin})_7/90_4/(\pm 25)_4/90_4/(\pm 35)_4/90_4/(\pm 45)_4]$ under four points bending loading

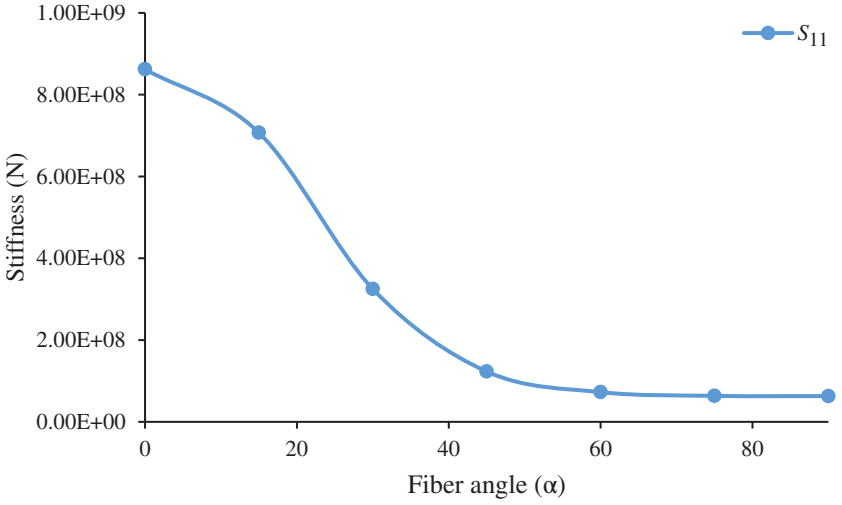

FIGURE 15 Extensional stiffness of the composite tube $[\pm\alpha_5]$ versus fiber angle (α)

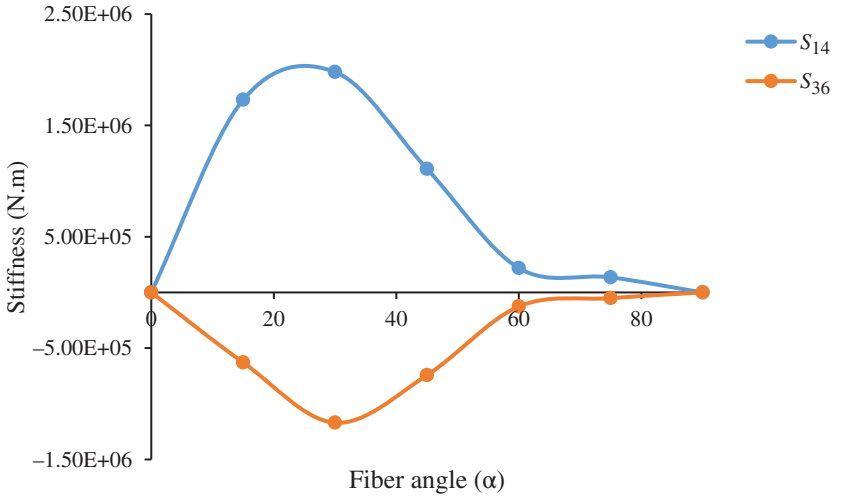

FIGURE 16 Extensional-torsional (S_{14}) and torsional-bending (S_{36}) stiffness of the composite tube $[\pm\alpha_5]$ versus fiber angle (α)

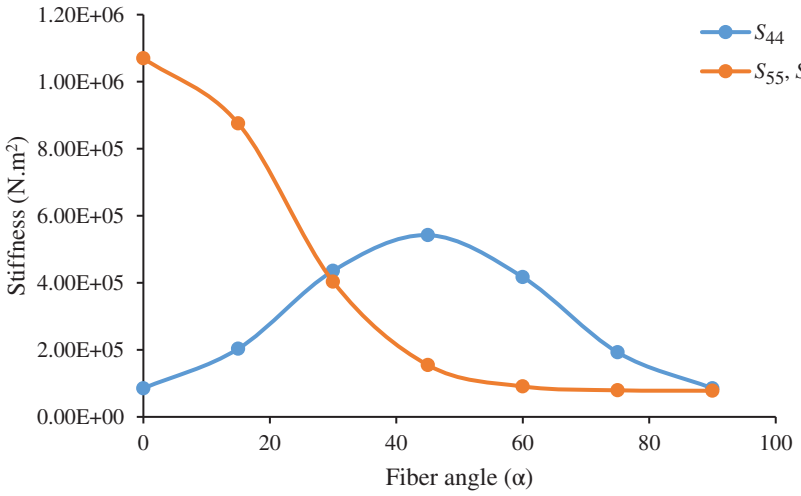

FIGURE 17 Torsional (S_{44}) and bending (S_{55}, S_{66}) stiffness of the composite tube $[\pm\alpha_5]$ versus fiber angle (α)

Figure 17 show that the torsional stiffness (S_{33}) is maximum at $\alpha = 45°$ and the bending stiffness (S_{55} and S_{66}) decreases by increasing the fiber angle.

5 | CONCLUSION

The conclusion can be made along two different aspects: The accuracy of the simple Pascal polynomial method, and the effect of the lay-up sequence on the need to use refined theory, as follows

- It was shown that the simple Pascal polynomial method can provide results that are as accurate as the VABS method and more computationally efficient than 3D FEA. This has been demonstrated for the determination of the stiffness constants, the through-section strains, and the deflection of the beam. This has also been demonstrated for tubes of different lay-up sequences, from simple lay-up sequence such as cross-plies to complicated lay-up sequences with different fiber angle orientations. For example, Section 5.3.1 shows the present cross-sectional analysis can substantially reduce the computational cost compared to 3D FEM. As such, the present method would be beneficial for structural optimization
- For tubes made of cross-ply layers, that is, $[0_m/90_n]$, there is no significant difference between the stiffness constants obtained using Classical model and Timoshenko model. This is due to the absence of shear coupling terms.

- In order to analyze cross-ply tubes, it is not necessary to use higher degree of the polynomial.
- For tubes with the lay-up sequence $[\pm\alpha_5]$, there is no difference between the obtained flexural stiffness of Classical and Timoshenko models.
- For tubes with lay-up sequence made of layers of different fiber orientation such as [45/15], there is a significant difference in the flexural stiffness of Timoshenko and Classical models obtained by both the Pascal polynomial method and VABS 3.8.
- To achieve higher precision of 3D strains for tubes with combination of angle ply layers, the order of applied polynomial needs to be increased, ($m \geq 5$).
- The extensional stiffness (S_{11}) decreases by increasing the fiber angle of a composite tube.
- The magnitude of extensional-torsional (S_{14}) and torsional-bending (S_{36}) of a composite tube are maximum at $\alpha = 30°$ of the fiber angle.
- The torsional stiffness (S_{33}) of a composite tube is maximum at $\alpha = 45°$ of the fiber angle.
- As the fiber angle increases, the bending stiffness (S_{55} and S_{66}) of a composite tube decreases.
- The present 1D FE formulation agrees well with 1D FE of ANSYS.

ACKNOWLEDGEMENTS

Financial support from the Natural Sciences and Engineering Research Council of Canada (NSERC) through the Industrial Research Chair on Automated Composites Manufacturing and from Bell Flight are appreciated.

NOMENCLATURE

a_i	Coefficients of the Pascal polynomial
$[A_1]$, $[A_2]$, $[A_3]$, $[A_4]$	Intermediate matrix expressions
$[C]$	Stiffness matrix in material coordinare system
$[D]$	Stiffness matrix in the beam coordinate system
E	Young modulus
e_i	Coordinates along principal material directions
$\boldsymbol{F}$	Vector of cross-sectional stress resultant
$[G]$, $[Y]$, $[X]$	Intermediate matrices
H	Beam thickness
I	Moment of inertia
J	Torsional moment of inertia
$[K^e]$	Element stiffness matrix
L	Beam length
L_e	Beam element length
$[M]$	Cross-sectional moment resultant vector
m	Order of the Pascal polynomial
p	Number of terms in the Pascal polynomial
r	Radial position of points in cross-section
$[S]$	6×6 Timoshenko stiffness cross-sectional matrix
$[\overline{S}]$	4×4 classical stiffness cross-sectional matrix
$[T]$	Element nodal coordinates matrix
$[T_\alpha]$, $[T_\beta]$	Transformation matrices
h	Tubular beam thickness
U_0, U_1	Approximations of the strain energy
U^e	Element strain energy
$\overline{u}, \overline{v}, \overline{w}$	Beam displacement components
w_1, w_2, w_3	Warping variables for cross-section
x_1, x_2, x_3	Coordinates of the structure
α	Fiber angle
$[\overline{\alpha}]$	Unknown coefficients matrix

β	Layer angle
γ_{12}, γ_{13}	Shear strains
γ_{11}	Extensional strain of the reference line in Timoshenko beam
$\overline{\gamma}_{11}$	Extensional strain of the reference line in Classical beam
$\boldsymbol{\delta}$	Nodal displacement vector
$\boldsymbol{\epsilon}$	Generalized Timoshenko strain vector
$\overline{\boldsymbol{\epsilon}}$	Generalized classical strain vector
$\epsilon_{\max}$	Maximum of 1D strains
θ	Circumferential angle
$\kappa_1, \kappa_2, \kappa_3$	Curvature variables in Timoshnko model
$\overline{\kappa}_1, \overline{\kappa}_2, \overline{\kappa}_3$	Curvature variables in classical model
$\overline{\varphi}_{x_1}, \overline{\varphi}_{x_2}, \overline{\varphi}_{x_3}$	Beam element rotations
$\boldsymbol{\psi}$	1D strain vector in Timoshenko beam model
Ω	Cross-section area
r_o	Outer radius of the cross-section

DATA AVAILABILITY STATEMENT

All data included in this study are available upon request by contact with the corresponding author. A brief data is also provided at https://users.encs.concordia.ca/~hoasuon/data/available_data.docx

ORCID

Suong Van Hoa https://orcid.org/0000-0002-4901-7212

REFERENCES

1. Derisi B. *Development of Thermoplastic Composite Tubes for Large Deformation* [Ph.D thesis]. Concordia University; 2008. https://spectrum.library.concordia.ca/976192/.
2. Giavotto V, Borri M, Mantegazza P, et al. Anisotropic beam theory and applications. *Comput Struct*. 1983;16(1):403-413.
3. Hodges DH. *Nonlinear Composite Beam Theory*. 213. USA: American Institute of Aeronautics and Astronautics; 2006. https://arc.aiaa.org/doi/book/10.2514/4.866821.
4. Yu W, Hodges DH, Ho JC. Variational asymptotic beam sectional analysis – an updated version. *Int J Eng Sci*. 2012;59:40-64.
5. Danielson DA, Hodges DH. Nonlinear beam kinematics by decomposition of the rotation tensor. *J Appl Mech*. 1987;54(2):258-262.
6. Wang Q, Yu W. Variational-asymptotic modeling of the thermoelastic behavior of composite beams. *Compos Struct*. 2011;93(9):2330-2339.
7. Yu W, Hodges DH, Volovoi V, Cesnik CES. On Timoshenko-like modeling of initially curved and twisted composite beams. *Int J Solids Struct*. 2002;39(19):5101-5121.
8. Berdichevsky V, Armanios E, Badir A. Theory of anisotropic thin-walled closed-cross-section beams. *Compos Eng*. 1992;2(5):411-432.
9. Hodges DH, Shang X, Cesnik CE. Finite element solution of nonlinear intrinsic equations for curved composite beams. *J Am Helicopter Soc*. 1996;41(4):313-321.
10. Popescu B, Hodges DH. On asymptotically correct Timoshenko-like anisotropic beam theory. *Int J Solids Struct*. 2000;37(3):535-558.
11. Cesnik CES, Hodges DH. VABS: a new concept for composite rotor blade cross sectional modeling. *J Am Helicopter Soc*. 1997;42(1):27-38.
12. Rehfield LW, Atilgan AR, Hodges DH. Nonclassical behavior of thin-walled composite beams with closed cross sections. *J Am Helicopter Soc*. 1990;35(2):42-50.
13. Ghafari E, Rezaeepazhand J. Isogeometric analysis of composite beams with arbitrary cross-section using dimensional reduction method. *Comput Methods Appl Mech Eng*. 2017;318:594-618.
14. Jiang F, Yu W. Nonlinear variational asymptotic sectional analysis of hyperelastic beams. *AIAA J*. 2016;54(2):679-690.
15. Harursampath D, Hodges DH. Asymptotic analysis of the non-linear behavior of long anisotropic tubes. *Int J Non-Linear Mech*. 1999;34(6):1003-1018.
16. Cesnik CE, Hodges DH, Sutyrin VG. Cross-sectional analysis of composite beams including large initial twist and curvature effects. *AIAA J*. 1996;34(9):1913-1920.
17. Stoer J, Bulirsch R. *Introduction to Numerical Analysis*. 12. Berlin, Germany: Springer Science & Business Media; 2013. https://www.springer.com/gp/book/9780387954523.
18. Sheikh AH, Thomsen OT. An efficient beam element for the analysis of laminated composite beams of thin-walled open and closed cross sections. *Compos Sci Technol*. 2008;68(10):2273-2281.
19. Seli H, Awang M, Ismail AIM, Rachman E, Ahmad ZA. Evaluation of properties and FEM model of the friction welded mild steel-Al6061-alumina. *Mater Res*. 2013;16(2):453-467.
20. Jolicoeur C, Cardou A. Analytical solution for bending of coaxial orthotropic cylinders. *J Eng Mech*. 1994;120(12):2556-2574.

21. Moshir SK, Hoa SV, Shadmehri F, Rosca D, Ahmed A. Mechanical behavior of thick composite tubes under four-point bending. *Compos Struct*. 2020;242:112097.
22. Shadmehri F, Derisi B, Hoa S. On bending stiffness of composite tubes. *Compos Struct*. 2011;93(9):2173-2179.

How to cite this article: Moshir SK, Hoa SV, Shadmehri F. Structural analysis of composite tubes using a meshless analytical dimensional reduction method. *Int J Numer Methods Eng*. 2021;122:3191–3217. https://doi.org/10.1002/nme.6660

APPENDIX A

$$[\overline{S}_{\text{Isotropic}}] = \begin{bmatrix} E\Omega & 0 & 0 & 0 \\ 0 & \text{GJ} & 0 & 0 \\ 0 & 0 & (\text{EI})_{x_2} & 0 \\ 0 & 0 & 0 & (\text{EI})_{x_3} \end{bmatrix} \tag{A1}$$

$$\begin{Bmatrix} \gamma_{11} \\ 2\gamma_{12} \\ 2\gamma_{13} \\ \kappa_1 \\ \kappa_2 \\ \kappa_3 \end{Bmatrix} = \begin{bmatrix} S_{11} & S_{12} & S_{13} & S_{14} & S_{15} & S_{16} \\ S_{12} & S_{22} & S_{23} & S_{24} & S_{25} & S_{26} \\ S_{13} & S_{23} & S_{33} & S_{34} & S_{35} & S_{36} \\ S_{14} & S_{24} & S_{34} & S_{44} & S_{45} & S_{46} \\ S_{15} & S_{25} & S_{35} & S_{45} & S_{55} & S_{56} \\ S_{16} & S_{26} & S_{36} & S_{46} & S_{56} & S_{66} \end{bmatrix}^{-1} \begin{Bmatrix} F_1 \\ F_2 \\ F_3 \\ M_1 \\ M_2 \\ M_3 \end{Bmatrix} \tag{A2}$$

$$[C] = \begin{bmatrix} \frac{1}{E_1} & 0 & 0 & -\frac{\nu_{21}}{E_2} & 0 & -\frac{\nu_{31}}{E_3} \\ 0 & \frac{1}{G_{12}} & 0 & 0 & 0 & 0 \\ 0 & 0 & \frac{1}{G_{13}} & 0 & 0 & 0 \\ -\frac{\nu_{12}}{E_1} & 0 & 0 & \frac{1}{E_2} & 0 & -\frac{\nu_{32}}{E_3} \\ 0 & 0 & 0 & 0 & \frac{1}{G_{23}} & 0 \\ -\frac{\nu_{13}}{E_1} & 0 & 0 & -\frac{\nu_{23}}{E_2} & 0 & \frac{1}{E_3} \end{bmatrix}^{-1} \tag{A3}$$

$$[T_\alpha] = \begin{bmatrix} \cos^2(\alpha) & 2\cos(\alpha)\sin(\alpha) & 0 & \sin^2(\alpha) & 0 & 0 \\ -\cos(\alpha)\sin(\alpha) & \cos^2(\alpha) - \sin^2(\alpha) & 0 & \cos(\alpha)\sin(\alpha) & 0 & 0 \\ 0 & 0 & \cos(\alpha) & 0 & \sin(\alpha) & 0 \\ \sin^2(\alpha) & -2\sin(\alpha)\cos(\alpha) & 0 & \cos^2(\alpha) & 0 & 0 \\ 0 & 0 & -\sin(\alpha) & 0 & \cos(\alpha) & 0 \\ 0 & 0 & 0 & 0 & 0 & 1 \end{bmatrix} \tag{A4}$$

$$[T_\beta] = \begin{bmatrix} 1 & 0 & 0 & 0 & 0 & 0 \\ 0 & \cos(\beta) & \sin(\beta) & 0 & 0 & 0 \\ 0 & -\sin(\beta) & \cos(\beta) & 0 & 0 & 0 \\ 0 & 0 & 0 & \cos^2(\beta) & 2\sin(\beta)\cos(\beta) & \sin^2(\beta) \\ 0 & 0 & 0 & -\sin(\beta)\cos(\beta) & \cos^2(\beta) - \sin^2(\beta) & \cos(\beta)\sin(\beta) \\ 0 & 0 & 0 & \sin^2(\beta) & -2\cos(\beta)\sin(\beta) & \cos^2(\beta) \end{bmatrix} \tag{A5}$$